

# Antimicrobial Peptide K<sup>0</sup>-W<sup>6</sup>-Hya1 Induces Stable Structurally Modified Lipid Domains in Anionic Membranes

Thais A. Enoki,<sup>\*,†,⊥</sup> Isabela Moreira-Silva,<sup>‡</sup> Esteban N. Lorenzon,<sup>§</sup> Eduardo M. Cilli,<sup>||</sup> Katia R. Perez,<sup>‡</sup> Karin A. Riske,<sup>‡</sup> and M. Teresa Lamy<sup>\*,†,||</sup>

<sup>†</sup>Instituto de Física da Universidade de São Paulo, São Paulo, SP, CEP 05508-090, Brasil

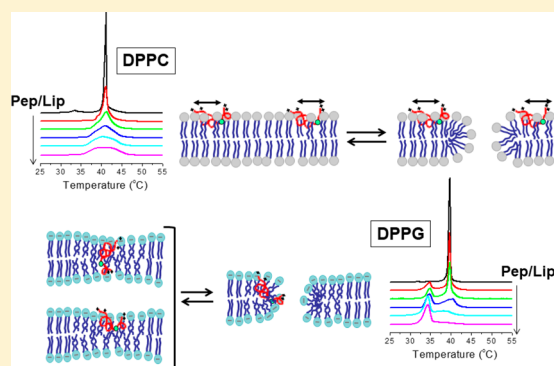
<sup>‡</sup>Departamento de Biofísica, Universidade Federal de São Paulo, São Paulo, SP, CEP 04039-032, Brazil

<sup>§</sup>Departamento de Bioquímica e Biologia Molecular, Instituto de Ciências Biológicas, Universidade Federal de Goiás, Goiânia, GO, CEP 74690-900, Brazil

<sup>||</sup>Instituto de Química, Universidade Estadual de São Paulo, Araraquara, SP, CEP 14800-060, Brazil

## S Supporting Information

**ABSTRACT:** Considering the known different mode of action of antimicrobial peptides in zwitterionic and anionic cell membranes, the present work compares the action of the antimicrobial peptide K<sup>0</sup>-W<sup>6</sup>-Hya1 (KIFGAIWPLALGALKNLIK-NH<sub>2</sub>) with zwitterionic and negatively charged model membranes, namely, liposomes composed of phosphatidylcholine (PC) and phosphatidylglycerol (PG) membranes, and a mixture of the two. Differential scanning calorimetry (DSC), steady state fluorescence of the Trp residue, dynamic light scattering (DLS), and measurement of the leakage of an entrapped fluorescent dye (carboxyfluorescein, CF) were performed with large unilamellar vesicles (LUVs). All techniques evidenced the different action of the peptide in zwitterionic and anionic vesicles. Trp fluorescence spectroscopy shows that the differences are related not only to the partition of the cationic peptide in zwitterionic and anionic membranes, but also to the different penetration depth of the peptide into the lipid bilayers: Trp goes deeper into negatively charged membranes, both in the gel and fluid phases, than into zwitterionic ones. DSC shows that the peptide is strongly attached to anionic bilayers, giving rise to the coexistence of two different lipid regions, one depleted of peptide and another one peptide-disturbed, possibly a stable or transient polar pore, considering the leakage of CF. This contrasts with the homogeneous effect produced by the peptide in zwitterionic membranes, probably related to peptide-membrane diffusion. Moreover, in mixed bilayers (PC:PG), the peptide sequesters negatively charged lipids, creating peptide-rich anionic lipid regions, strongly disturbing the membrane. The distinct structural interaction displayed by the peptide in PC and PG membranes could be related to the different mechanisms of action of the peptide in anionic prokaryotic and zwitterionic eukaryotic cell membranes.



## 1. INTRODUCTION

Antimicrobial peptides (AMPs) are important molecules in the innate immune defense system of plants and animals.<sup>1,2</sup> Due to the growth of pathogen microorganisms resistant to conventional antibiotics,<sup>3</sup> there is an urgent need for the development of antibiotics with new mechanisms of action. Several studies have pointed out antimicrobial peptides as an efficient alternative.

Even though hundreds of AMPs have been reported with a diversity of sequences, they show a few common properties. For instance, it is well accepted that their mechanism of action involves cell membrane disruption, and does not involve any receptor-mediated pathway, thus hindering the development of AMPs-resistant microorganisms. In general, these peptides are cationic, with 10–50 amino acid residues, including polar and nonpolar, which allow them to adopt an amphipathic conformation. In addition, AMPs can exhibit different and

highly complex mechanisms of action. Their ability to disrupt the structural integrity of membranes has been attributed to diverse phenomena: pore formation (barrel-stave or toroid pores),<sup>4,5</sup> membrane disintegration as detergent-like action (carpet model),<sup>6,7</sup> formation of peptide-lipid domains,<sup>8,9</sup> segregation of anionic lipids,<sup>10,11</sup> or formation of nonlamellar phases.<sup>12,13</sup>

The electrostatic interaction plays an important role in the interaction of AMPs with cell membranes. Due to their positive charges, AMPs are usually found to be much more toxic against bacterial cells, because of their negatively charged surface, than against zwitterionic mammalian cells. Considering the complexity of natural membranes, and to allow the study of the

Received: September 28, 2017

Revised: December 24, 2017

Published: December 28, 2017

structural effects caused by AMPs in lipid bilayer domains, model lipid membranes have been extensively used.<sup>14</sup> Usually, phosphatidylcholine (PC) membranes are used to mimic zwitterionic mammalian membranes, and the anionic phosphatidylglycerol (PG), which is found in abundance in bacterial membranes, or a mixture of PC–PG, are used to mimic the outer leaflet of bacterial membranes.

Here, we study the antimicrobial peptide K<sup>0</sup>-W<sup>6</sup>-Hya1, which displays antimicrobial and antifungal actions,<sup>15,16</sup> the first against both Gram-positive and Gram-negative bacteria. This peptide (KIFGAIWPLALGALKNLK-NH<sub>2</sub>) is an analogue of the peptide Hylin a1,<sup>17</sup> isolated from the skin secretion of the frog *Hypsiboas albopunctatus*. In K<sup>0</sup>-W<sup>6</sup>-Hya1, a Leu was replaced by Trp at the sixth position, and a Lys was inserted at the first position. The insertion of an additional positively charged amino acid at the N-terminus has improved its antimicrobial and antifungal properties, but also increased its hemolytic activity.<sup>15</sup> Due to the amidated C-terminus, the peptide exhibits a net charge of +4 at neutral pH (Figure S1 of Supporting Information). Previous studies showed that this peptide is not structured in aqueous medium and acquires a certain amount of  $\alpha$  helix structure in the presence of lysolecithin micelles.<sup>15</sup>

We investigate the interaction of K<sup>0</sup>-W<sup>6</sup>-Hya1 with large unilamellar vesicles (LUVs) composed of the zwitterionic DPPC (1,2-dipalmitoyl-*sn*-glycero-3-phosphocholine), to mimic mammalian membranes, and of anionic DPPG (1,2-dipalmitoyl-*sn*-glycero-3-phospho-(1'-*rac*-glycerol)), or a mixture of DPPC-DPPG, to model the outer leaflet of bacterial membranes. Saturated lipids were used in the gel and fluid phases of the membrane, to mimic both more packed and less packed lipid domains, respectively. Moreover, with saturated lipids, it was possible to follow the gel–fluid bilayer transition by differential scanning calorimetry (DSC), which can give information about the peptide–membrane binding, and membrane structural alterations. With those lipid systems, DSC, steady state fluorescence of the Trp residue, and dynamic light scattering (DLS) were performed. Furthermore, measurement of the leakage of entrapped carboxyfluorescein (CF), a fluorescent dye, was performed with LUVs of DPPC, DPPG and DPPC:DPPG in the gel phase, at 25 °C, and with similar systems, but in the fluid phase at 25 °C, namely, POPC (1-palmitoyl-2-oleoyl-*sn*-glycero-3-phosphocholine), POPG (1-palmitoyl-2-oleoyl-*sn*-glycero-3-phospho-(1'-*rac*-glycerol)), and POPC:POPG. The peptide Trp fluorescence was also monitored in the nonsaturated lipid systems.

All techniques indicate that the peptide causes different structural alterations in zwitterionic and negatively charged membranes. The peptide partitions, penetrates and disrupts zwitterionic membranes, but it is possibly located close to the surface of the membrane, and diffuses over the surface. In contrast, in anionic bilayers, Trp in K<sup>0</sup>-W<sup>6</sup>-Hya1 is in a position deeper into the membrane, both in the gel and fluid phases, and stable peptide-lipid domains can be detected by DSC, which are probably related to bilayer pores, as indicated by CF leakage.

## 2. EXPERIMENTAL SECTION

**2.1. Chemicals and Reagents.** DPPG (1,2-dipalmitoyl-*sn*-glycero-3-phospho-(1'-*rac*-glycerol) - sodium salt), DPPC (1,2-dipalmitoyl-*sn*-glycero-3-phosphocholine), POPG (1-palmitoyl-2-oleoyl-*sn*-glycero-3-phospho-(1'-*rac*-glycerol) - sodium salt), and POPC (1-palmitoyl-2-oleoyl-*sn*-glycero-3-phosphocholine) were obtained from Avanti Polar Lipids (Alabaster, AL). HEPES (4-(2-hydrox-

yethyl)-1-piperazineethanesulfonic acid), EDTA (ethylenediaminetetraacetic acid disodium salt), NaCl (sodium chloride), CF (5(6)-carboxyfluorescein, purified as described in ref 18), and Triton-X100 were obtained from Sigma-Aldrich (St Louis, MO).

**2.2. Peptide Synthesis.** The peptide was synthesized manually using the Fmoc strategy, purified, and characterized according to the experimental protocol used before.<sup>15</sup>

**2.3. Peptide–Lipid Dispersions Preparation.** Lipids were dissolved in chloroform and dried under a stream of N<sub>2</sub>, forming a lipid film at the bottom of the glass tube. The film was left under low pressure for 3 h to remove all traces of organic solvent. Aqueous dispersions were prepared by the addition of 10 mM HEPES buffer pH 7.4 with 1 mM EDTA and 3 mM NaCl to the lipid film, followed by vortexing during 2 min at 45 °C. After that, lipid dispersions were extruded through polycarbonate filters (mini-extruder by Avanti Polar Lipids, 19 mm membranes with 100 nm pores, 31 times) above the lipid gel–fluid transition temperature, for the formation of large unilamellar vesicles (LUVs).

Peptides were added after LUVs formation, at room temperature. The peptide-lipid molar ratio [P]/[L] corresponds to the ratio between peptide and lipid total molar concentrations, [P] and [L], respectively. The lipid concentration was determined by inorganic phosphate assay,<sup>19</sup> where L stands for DPPC, DPPG and DPPG:DPPC (1:1, mol:mol). For optical absorption, fluorescence and DLS studies, samples with increasing [P]/[L] ratios were prepared by the subsequent addition of a concentrated peptide solution, with the necessary volume correction. For DSC and leakage of entrapped dye experiments, each [P]/[L] sample was prepared independently.

**2.4. Differential Scanning Calorimetry.** Calorimetric measurements were carried out with a microcalorimeter (Microcal VP-DSC, Northampton, MA). Samples were heated from 15 to 50 °C at a scan rate of 20 °C/h. The sample cell (~500  $\mu$ L) was filled with a 3 mM lipid dispersion with the addition of the desired concentration of peptide. Baseline subtractions and peak integrals were performed using the MicroCal Origin software with the additional module for DSC data analysis provided by MicroCal, as previously described.<sup>20</sup> For all systems used, scans shown here are typical profiles obtained from at least two identically prepared samples.

**2.5. Optical Absorption Spectroscopy.** Optical absorption spectra were obtained with an UV–vis spectrophotometer (Varian Cary, Santa Clara, CA). Samples were placed in a quartz cuvette (0.2  $\times$  1.0 cm), with the absorption optical pathway of 1.0 cm. The temperature was controlled with a Cary Peltier thermostat, and measurements were performed at 25 and 50 °C. The peptide concentration in the stock solution was obtained from the Trp absorption at  $\lambda = 280$  nm, using an extinction coefficient  $\epsilon = 5500$  (cm<sup>-1</sup>·M<sup>-1</sup>) (ref 21 and references therein). Lipid concentration was 0.5 mM.

Typical optical absorption spectra of samples at different [P]/[L] concentrations are shown in Figure S2. Not only the Trp absorption band increases ( $\lambda = 280$  nm, (1) in Figure S2) as the peptide concentration increases, but also the scattering background (for instance, see region (2) in Figure S2). For higher peptide concentration, [P]/[L] = 0.08, light scattered by the dispersion was found to increase significantly, hence we decided to work up to [P]/[L] = 0.07.

**2.6. Fluorescence Spectroscopy.** The Trp emission spectrum ( $\lambda_{\text{exc}} = 280$  nm) was measured with a fluorescence spectrometer (Varian Cary Eclipse, Santa Clara, CA). Samples containing 500  $\mu$ L of lipid dispersion (0.5 mM), without or with peptide, were placed in quartz cuvettes (0.2  $\times$  1.0 cm), and the temperature was controlled using a Cary Peltier thermostat.

Here, we briefly describe the applied inner filter corrections, to obtain accurate parameters from the spectra: emission intensity and wavelength of maximal emission. As previous reported,<sup>22,23</sup> fluorescent emission must be corrected considering the decrease in the intensity of light reaching the emitting fluorophores at the center of the cuvette, due to light absorbance or scattering (primary inner filter correction; see arrow (1) in Figure S2). Moreover, as discussed above, there is an increase in scattered light with the increase in peptide concentration.

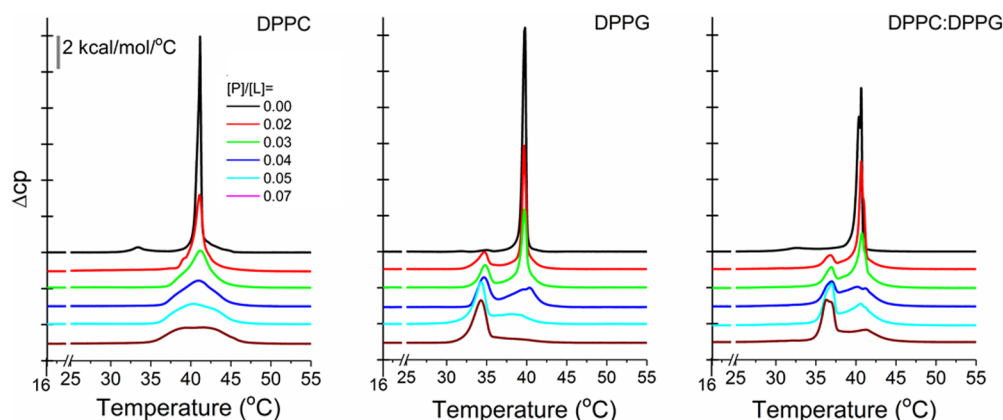


**Figure 1.** DSC of extruded lipid dispersions composed by DPPC, DPPG, and the mixture DPPC:DPPG (black line), and dispersions with increasing peptide–lipid molar ratio,  $[P]/[L] = 0.02, 0.03, 0.04, 0.05,$  and  $0.07$ . Scans were obtained using a scan rate of  $+20$  °C/h, and they are shifted for clarity. Duplicate samples showed similar results.

Hence, a second correction is necessary (second inner filter correction), which considers the decrease in the measured fluorescent emission due to light scattering (see arrow (2) Figure S2). An example of the relevance of the corrections discussed above can be seen in Figure S3 (Supporting Information).

The inner filter correction (eq 1) was applied after the blank (buffer, or lipid dispersion) subtraction:

$$F(\lambda) = F_0(\lambda)10^{(A_{\text{exc}}x)}10^{(A_{\text{em}}x')} \quad (1)$$

where  $F_0(\lambda)$  and  $F(\lambda)$  are the measured and the corrected fluorescence intensities, respectively.  $A_{\text{exc}}$  and  $A_{\text{em}}$  are the absorbance values per unit of optical pathway at the excitation and emission wavelengths, respectively.  $A_{\text{exc}}$  was measured at 280 nm, and  $A_{\text{em}}$  varied with the emission wavelength. The optical pathway for excitation was  $x = 0.1$  cm, and for the emission  $x' = 0.5$  cm (half of the cuvette optical pathways). Equation 1 does not consider the dimensions of the excited region, as it is assumed that all emitting fluorophores are at the center of the cuvette. Mendonça et al.<sup>23</sup> showed that this equation is suitable for the absorbance values obtained here.

**2.7. Dynamic Light Scattering.** DLS measurements were performed in a Zetasizer Malvern (Nano ZS, Worcestershire, UK). The autocorrelation function of the intensity of the scattered light,  $g^{(2)}(\tau)$ , is directly obtained by a digital correlator, and it is related to the electric field autocorrelation function  $g^{(1)}(\tau)$  by the Siegert relation:<sup>24</sup>

$$g^{(2)}(\tau) = 1 + \beta |g^{(1)}(\tau)|^2 \quad (2)$$

Here, autocorrelation functions were obtained at 90°, and  $g^{(1)}(\tau)$  analyzed by the Method of Cumulants<sup>25</sup> of second order:

$$\langle g^{(1)}(\tau) \rangle = \exp\{-\langle \Gamma \rangle \tau + \mu_2 \tau^2 / 2!\} \quad (3)$$

where  $\mu_2$  is the second-order moment of the expansion, related to the system polydispersity, and  $\langle \Gamma \rangle$  is the average decay rate or relaxation frequency.  $\langle \Gamma \rangle$  is related to the particle  $z$ -average translational diffusion coefficient ( $D_T$ ) and the scattering vector, according to eq 4:

$$\langle \Gamma \rangle = D_T q^2 \quad (4)$$

where  $q = 4\pi \sin(\theta/2)/\lambda$  and  $\theta$  is the scattering angle.<sup>24</sup> To reduce vesicle–vesicle interaction, as it can distort the calculated vesicle translational diffusion coefficient, a low lipid concentration was used (0.1 mM).<sup>26</sup>

By modeling the scattering centers as spheres, their effective hydrodynamic radius ( $R_{\text{eff}}$ ) can be obtained from the translational diffusion coefficient  $D_T$ , according to the Stokes–Einstein equation:

$$D_T = (k_B T) / (6\pi\eta R_{\text{eff}}) \quad (5)$$

where  $k_B$  is the Boltzmann constant,  $T$  is the absolute temperature, and  $\eta$  is the solvent viscosity.

**2.8. Entrapment of Carboxyfluorescein (CF) in LUVs and Leakage Assay.** Lipid films were hydrated with buffer containing 50 mM carboxyfluorescein. The lipid dispersion was extruded, as described above. To remove nonentrapped CF, the suspension of LUVs was eluted through a Sephadex-G25 medium column (1.2 cm  $\times$  20 cm) with 10 mM HEPES, pH 7.4 with 1 mM EDTA, 3 mM NaCl and 150 mM glucose, the latter added to adjust the osmolarity inside and outside liposomes. Vesicles with entrapped CF (CF-LUVs) were collected in the void volume of the column. Lipid dispersions were prepared at 10 mM. After the elution through the Sephadex column we obtained a 4 to 5-fold dilution. The final lipid concentration was determined by inorganic phosphate assay.<sup>19</sup>

Samples were placed in quartz cuvettes (1.0  $\times$  1.0 cm, 1.0 mL) and the fluorescent emission measured with a Fluorescence Spectrometer (Varian Cary Eclipse, Santa Clara, CA), with temperature controlled by a Carry Peltier thermostat. The CF leakage measurements were performed under constant stirring. In the cuvette, we placed 40  $\mu$ L of the lipid dispersion, and the final lipid concentration was found to range between 60–150  $\mu$ M, after the inorganic phosphate assay. The CF entrapped in liposomes is self-quenched at the concentration used here (50 mM). As CF is released to the bulk solution, due to membrane permeabilization caused by the peptide or detergent addition, the fluorophore is diluted and its fluorescent signal increases. CF emission was continuously recorded in time (one measurement per second), at 25 °C,  $\lambda_{\text{exc}} = 490$  nm and  $\lambda_{\text{em}} = 512$  nm. Different concentrations of peptide were added to the LUV dispersions. At the end of each experiment (2000 s), Triton X-100 was added (25  $\mu$ L of 10% w/v) to promote full CF leakage.

The percentage of CF leakage, (%)leakage, was determined according to eq 6:

$$(\%) \text{leakage}(t) = [(I(t) - I_0) / (I_{\text{total}} - I_0)] \times 100 \quad (6)$$

where  $I(t)$  is the fluorescence intensity at time  $t$ ,  $I_0$  is the initial fluorescence, before peptide addition, and  $I_{\text{total}}$  is the maximum fluorescence, obtained after the addition of Triton X-100.<sup>27</sup>

The kinetics were performed with vesicles of DPPC, DPPG, and DPPC:DPPG in the gel phase only, at 25 °C, as the experimental procedure at 50 °C was found rather unreliable, with CF leaking considerably from vesicles even in the absence of peptide. That could be due to the difficulty of keeping the sample above  $T_m$ , temperature at which vesicles are known to become leaky. To mimic the fluid phase of the dipalmitoyl membranes, similarly prepared vesicles of POPC, POPG, and POPC:POPG were used at 25 °C.

All data shown are means of at least three experiments, and uncertainties are calculated standard deviations. If not shown, the uncertainty was found to be smaller than the graphic symbol.

### 3. RESULTS

The interaction of the antimicrobial peptide  $K^0$ -W<sup>6</sup>-Hya1 with model membranes, composed of zwitterionic and negatively charged lipids, was studied using different techniques: DSC, Trp fluorescence, DLS, and leakage of the fluorophore carboxyfluorescein (CF) entrapped in LUVs. As the saturated lipids DPPC and DPPG display a gel–fluid transition around 40 °C, it was possible to study peptide–lipid interaction in both gel (more rigid/organized) and fluid membranes, by temperature variation, and the effect of the peptide on the bilayer thermal transition. The leakage of CF was performed at 25 °C, with LUVs of DPPC, DPPG, and DPPC:DPPG (1:1; mol:mol) in the gel phase, and with POPC, POPG, and POPC:POPG (1:1; mol:mol) in the fluid phase. The fluorescence of Trp (in the seventh position of the peptide chain; see Figure S1) was used to monitor the insertion depth of this residue into the bilayer. DLS gives the average hydrodynamic radius of the liposome-peptide bound system, informing about liposome-liposome aggregation or fusion, and bilayer disruption was monitored via the extent of CF leakage.

**3.1. Differential Scanning Calorimetry.** The thermal phase transition of a lipid bilayer depends on lipid–lipid interaction, and can be very sensitive to the presence of an exogenous molecule, informing about structural characteristics of molecule–lipid interaction. Figure 1 compares DSC profiles of pure LUVs dispersions (black) of zwitterionic DPPC, anionic DPPG and the mixture DPPC:DPPG (1:1, mol:mol), with those of LUVs with increasing peptide molar ratio,  $[P]/[L]$ . For pure lipids, similar to nonextruded dispersions,<sup>20</sup> the pre ( $T_p$ ) and the main ( $T_m$ ) transition temperatures of DPPC and DPPG were found at  $T_p = 33.5 \pm 0.1$  °C and  $34.8 \pm 1.2$  °C, and  $T_m = 41.1 \pm 0.1$  °C and  $39.5 \pm 0.1$  °C, respectively, and their associated enthalpies  $\Delta H_p \approx 0.6$  kcal/mol and  $\Delta H_m \approx 8.0$  kcal/mol, for both lipids (see Figure S4 and Table S1 in the Supporting Information). The transition temperatures for the mixture DPPC:DPPG were found to be  $T_p = 32.4 \pm 0.4$  °C and  $T_m = 40.3 \pm 0.4$  °C, with the latter in between those found for DPPC and DPPG, and with similar enthalpy value,  $\Delta H_m \approx 8.0$  kcal/mol. The two lipids are probably randomly distributed in the membrane in an ideal mixture.<sup>28</sup>

DSC profiles show distinct effects of the peptide in membranes of zwitterionic (DPPC) and in those of negatively charged lipids (DPPG and DPPC:DPPG). The increase in  $[P]/[L]$  molar ratio progressively broadens the main transition of DPPC, indicating a decrease in the cooperativity of the lipid phase transition. Thus, these profiles suggest a homogeneous perturbation of the lipids due to peptide binding.

On the other hand, DSC profiles of DPPG and DPPC:DPPG show that as the  $[P]/[L]$  molar ratio increases, a new thermal event grows up, centered at  $T = 34.0 \pm 0.1$  and  $36.5 \pm 0.1$  °C, respectively. Interestingly, for low values of  $[P]/[L]$ , 0.02 and 0.03, an approximately pure lipid gel–fluid transition peak coexists with the new thermal event, clearly indicating the coexistence of peptide-bound and peptide-free regions in the bilayer. As the peptide concentration increases ( $[P]/[L] = 0.04, 0.05$  and  $0.07$ ), the magnitude of the peak at lower temperatures increases as the other one broadens. With peptide addition, the total enthalpy of the gel–fluid transition (including the two thermal events for DPPG or the broadening of the DPPC peak) slightly decreases, whereas for DPPC:DPPG the enthalpy remains roughly the same as that obtained for pure lipids (see Table S2). It is noticeable that

even the lowest peptide concentration,  $[P]/[L] = 0.02$ , causes the vanishing of the pretransition in the three lipid systems used here, DPPC, DPPG, and DPPC:DPPG (see Figure 1).

Figure 2 shows up-scans and down-scans and down-scans for some of the samples (Figure S5 shows the scans for all  $[P]/[L]$  ratios

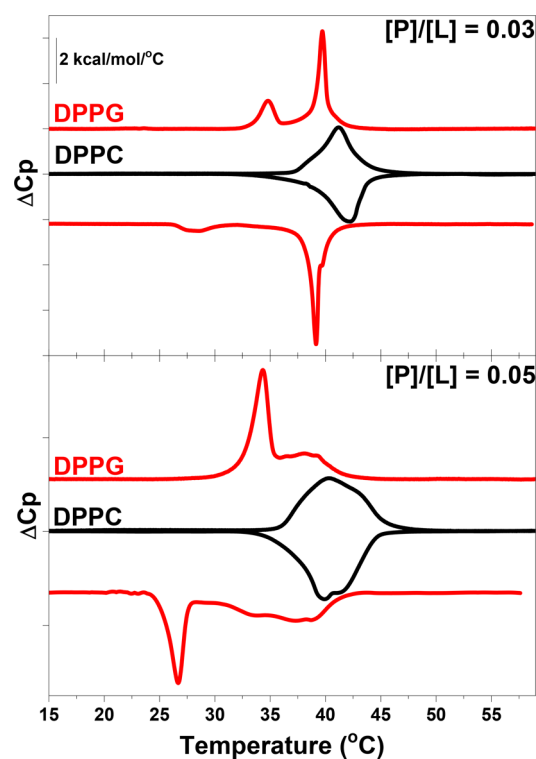


**Figure 2.** Up and down DSC scans for DPPC (black) and DPPG (red), with two different  $[P]/[L]$  ratios. A temperature up-scan was followed by a temperature down-scan. DPPG traces are shifted for better visualization.

studied). The temperature scans for the three pure lipid systems show that their thermal transitions are not only reproducible but also reversible (Figure S5). Also reversible are the thermal transitions for DPPC-peptide bound bilayers, supporting the assumption of  $K^0$ -W<sup>6</sup>-Hya1 causing a homogeneous effect on the bilayer (Figures 2 and S5). For anionic lipids, with low  $[P]/[L]$  ratio, 0.03 (Figure 2), the coexistence of bulk lipids and peptide-bound lipid domains is also observed in the temperature down-scan. Interestingly, bulk DPPG membrane displays a rather reversible thermal transition, but peptide-DPPG domains display a significant hysteresis ( $\sim 7$  °C). The presence of the two lipid domains, with different transition temperatures, in both heating and cooling scans, is a strong evidence of the formation of peptide–lipid domains both in the gel and fluid phases. Accordingly, these peptide-disturbed lipids in the fluid phase need a lower temperature to get more organized in a gel phase.

**3.2. Trp Fluorescence Spectroscopy.** The Trp residue, at the seventh position of the peptide chain, is a good probe to monitor the peptide behavior in liposome dispersions, as Trp fluorescence spectrum is extremely sensitive to the fluorophore environment. Figure 3 shows typical Trp emission spectra (obtained after the spectrum corrections discussed in Section 2.6), for the peptide in HEPES buffer and in the presence of fluid bilayers of DPPC, DPPG and DPPC:DPPG, for different peptide concentrations, at  $T = 50$  °C. (Spectra were also

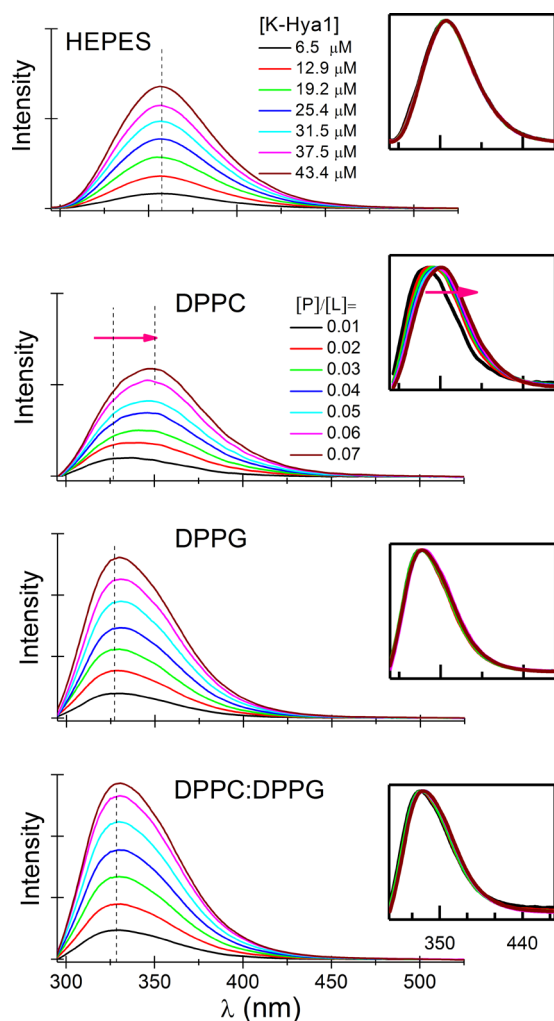


**Figure 3.** Emission spectra of peptide  $K^0-W^6$ -Hya1 in HEPES buffer and in lipid dispersions of DPPC, DPPG and DPPC:DPPG, at the peptide-lipid molar ratios  $[P]/[L] = 0.01, 0.02, 0.03, 0.04, 0.05, 0.06$  and  $0.07$ , at  $T = 50^\circ\text{C}$  (membrane fluid phase). Spectra were corrected for the inner filter effect as discussed in the [Experimental Section](#). Dotted lines indicate the wavelength of maximal emission, and insets show the normalized spectra. The vertical spacing represents 200 au in the intensity axis.  $\lambda_{\text{exc}} = 280\text{ nm}$ .

obtained at  $25^\circ\text{C}$ , with the lipids in the gel phase, and similar corrections were performed, [Figure S6](#), Supporting Information). Inserts at the right side of the graphs display the normalized spectra. For the four systems, the shape of the spectra does not change with the increase of the peptide concentration, but in DPPC there is a red shift as  $[P]/[L]$  increases (see dotted lines in [Figure 3](#)).

[Figure 4](#) shows the effect of the  $[P]/[L]$  ratio in the intensity of the Trp emission (the integral of the emission band, A and B) and in the blue shift of the wavelength of maximal emission ( $\Delta\lambda_{\text{max}} = \lambda_{\text{max}}^{\text{HEPES}} - \lambda_{\text{max}}^{\text{lipid}}$ , C and D) for the peptide in the four situations, at the two temperatures, 25 and  $50^\circ\text{C}$ .

First, it is important to note that the intensity of the Trp emission spectra increases almost linearly with the peptide concentration, for all systems, as displayed in [Figure 4A](#) and B. (There is possibly a deviation from linearity for DPPC:DPPG with  $[P]/[L] = 0.07$ . However, a significant light scattering is observed in this case, as shown in [Figure S7](#), and hence, the applied spectra corrections could be inadequate.) These results

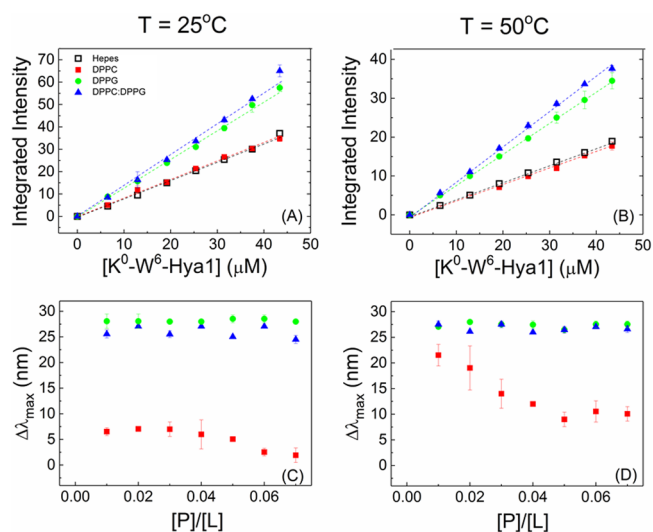


**Figure 4.** Effect of the peptide concentration on the emission spectrum intensity (A and B) of  $K^0-W^6$ -Hya1 ( $\lambda_{\text{exc}} = 280\text{ nm}$ ) in HEPES (black open squares) and in lipid dispersions of DPPC (red squares), DPPG (green circles) and DPPC:DPPG (blue triangles), at  $25^\circ\text{C}$  (lipids gel phase) and  $50^\circ\text{C}$  (lipids fluid phase). Integrated Intensities of  $K^0-W^6$ -Hya1 emission spectrum are plotted as a function of the peptide concentration to evidence its linear dependence on  $[P]$ . (C and D) Effect of the peptide concentration on the shift of the Trp fluorescent band relative to the band in HEPES ( $\Delta\lambda_{\text{max}} = \lambda_{\text{max}}^{\text{HEPES}} - \lambda_{\text{max}}^{\text{lipid}}$ ) in lipid dispersions of DPPC (red squares), DPPG (green circles), and DPPC:DPPG (blue triangles), at 25 and  $50^\circ\text{C}$ .

suggest that there is no Trp-Trp contact for the peptide concentrations used here, neither in solution nor in the bilayers, as, usually, the interaction between chromophores leads to change in their energy levels, hence in their absorption and/or emission spectrum.<sup>29</sup> Similar linear behavior was obtained with Trp absorbance values at 280 nm ([Figure S8](#)).

For zwitterionic DPPC, the intensity of the Trp emission is very similar to that observed for the peptide in aqueous solution, but  $\lambda_{\text{max}}$  shifts to shorter wavelengths, a clear indication of peptide-membrane interaction, with Trp embedded in a less polar environment. The shift is more pronounced for the membrane fluid phase ( $50^\circ\text{C}$ ) than for the gel phase ( $25^\circ\text{C}$ ), and it is more evident for lower  $[P]/[L]$  ratios. For instance, for  $[P]/[L] = 0.01$ ,  $\Delta\lambda_{\text{max}} \sim 22$  and  $\sim 7\text{ nm}$ , for the fluid and gel phases, respectively. That difference in the wavelength of maximal emission might be related to a deeper penetration of the peptide, hence of Trp, into the bilayer hydrophobic core for the fluid phase, as compared with the bilayer gel phase. That is expected, as the fluid phase is characterized by a larger area per lipid, due to the increase of lipid chains disorder, usually allowing deeper penetration of exogenous molecules.<sup>30</sup>

In DPPC, for both lipid phases (at 25 and  $50^\circ\text{C}$ ), the emission band gradually moves to longer wavelengths with increasing peptide molar ratio (see the decrease in  $\Delta\lambda_{\text{max}}$  in [Figure 4C](#) and D), getting closer to the position of the emission band for the peptide free in buffer. That can be attributed to a gradual change in the Trp environment, hence in the peptide location in the membrane, as the peptide concentration in the membrane increases. However, there is a second interpretation that we favor: as  $[P]/[L]$  increases, the concentration of peptide bound to the membrane increases, leading to a more cationic membrane, with structural changes, thus the affinity of

the positively charged peptide for the bilayer decreases. Therefore, the amount of peptide-bound to the membrane tends to saturate as the peptide concentration increases, and relatively more peptide would go to buffer. That is more evident for the membrane in its fluid phase, at 50 °C (Figure 4D), either because the peptide (the Trp residue) inserts deeper into the fluid bilayer, or because peptide–membrane partition is higher for fluid membranes at lower peptide concentration.

Accordingly, in DPPC, both in the gel and fluid phases (25 and 50 °C), the emission spectrum of Trp would be a composition of two bands, related to the fluorophore in buffer ( $\lambda_{\text{max}} \approx 357$  nm) and in DPPC bilayer ( $\lambda_{\text{max}} \approx 350$  and 335 nm, for the gel and fluid phases, respectively). The increase in  $[P]/[L]$  ratio would increase the relative amount of free peptide, increasing the relative intensity of the peptide spectrum in buffer, as compared to the spectrum in the lipid bilayer, decreasing the blue shift of the total emission spectrum. For instance, the Trp emission spectrum for  $[P]/[L] = 0.07$  in DPPC, at 50 °C, can be roughly reproduced as a composition of the Trp spectrum in HEPES buffer and that obtained at  $[P]/[L] = 0.01$  (Figure S9). The latter is the spectrum shown here closest to that yielded if all peptide would be in the bilayer. As the Trp fluorescence intensity in DPPC and in water medium are rather similar (Figure 4A and B), even with the decrease in the peptide–membrane partition coefficient as  $[P]$  increases, we expect a linear variation of the fluorescence intensity with  $[P]$ , as observed in Figure 4A and B.

In contrast, the interaction of peptide  $K^0$ -W<sup>6</sup>-Hya1 with negatively charged lipid bilayers (DPPG and DPPC:DPPG) leads to a significant blue shift of the emission peak,  $\Delta\lambda_{\text{max}} \approx 27$  nm, for both gel and fluid lipid phases, at all peptide concentrations (Figure 4C and D). Therefore, Trp senses a quite hydrophobic environment, and the concentration of peptide free in solution seems to be negligible for all peptide concentrations used here. In accordance with a more hydrophobic environment for Trp in anionic membranes, Trp fluorescence intensity increases considerably, compared to the intensity in aqueous medium or DPPC.

**3.3. Dynamic Light Scattering.** To monitor possible vesicle–vesicle aggregation or fusion, or any alteration in vesicle dimensions with the addition of peptide to the lipid dispersion, measurements of dynamic light scattering (DLS) were performed to characterize the dimensions of the scattering centers. Figure 5 shows the effective radius,  $R_{\text{eff}}$ , of the particles

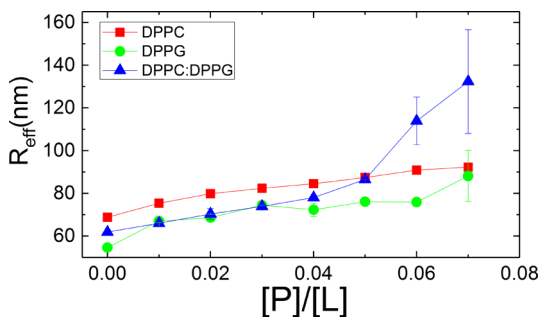


**Figure 5.** Effective radii  $R_{\text{eff}}$  for lipid dispersions DPPC (red squares), DPPG (green circles), and DPPC:DPPG (blue triangles) as a function of the peptide molar ratio  $[P]/[L] = 0.01, 0.02, 0.03, 0.04, 0.05, 0.06,$  and  $0.07$ . Data were collected at  $T = 25$  °C (gel lipid phase). Errors for two independent set of samples are represented.

in DPPC, DPPG, and DPPC:DPPG dispersions as a function of peptide concentration, at  $T = 25$  °C. We observe an increase in  $R_{\text{eff}}$  as the peptide concentration increases, for all studied lipid systems. For  $[P]/[L] = 0.07$ ,  $R_{\text{eff}}$  increases  $\sim 30\%$  for DPPC,  $\sim 60\%$  for DPPG, and  $\sim 100\%$  for the mixture DPPC:DPPG. This is in accord with the increase in the intensity of scattered light by the dispersions with the increase in peptide concentration, as mentioned before (Figure S7).

As an example, DPPC shows an increase of 30% in a sphere radius leading to an increase of  $\sim 70\%$  in the vesicle area, which could hardly be caused by just the insertion of the peptide into the DPPC bilayer. Even for DPPC dispersions, there is a mild extension of vesicle–vesicle aggregation, or fusion, for the highest concentrations of peptide. It should be noted that a small percent of large particles can lead to a significant increase in the effective radius, since it is a z-average effective radius.<sup>24</sup> It is also important to mention that no precipitate was observed during the time course of the experiment.

**3.4. Carboxyfluorescein (CF) Leakage Assay.** Considering that antimicrobial peptides are known to change the structure of cell membranes, altering their permeability (see, for instance, refs 15–18), the ability of the peptide  $K^0$ -W<sup>6</sup>-Hya1 to change the permeability of zwitterionic and anionic membranes was investigated with fluorescence spectroscopy through experiments of leakage of CF encapsulated in LUVs.

The leakage kinetics are shown in Figure 6, for the different  $[P]/[L]$  ratios, in DPPC, DPPG, and DPPC:DPPG, at 25 °C, in the lipid gel phase, and with POPC, POPG, and POPC:POPG, at 25 °C, to mimic the fluid phase of the dipalmitoyl lipid systems (see Experimental Section). The spontaneous CF leakage through lipid membranes in the absence of peptide was found to be negligible (in 30 min, less than 1% and 10%, for gel and fluid vesicles, respectively), and is shown in Figure 6 (black lines). Peptides are injected at the time signaled by arrow (1), and Triton X-100 is added at the end (arrow 2), to promote full CF leakage.

In both zwitterionic and anionic liposomes, the peptide  $K^0$ -W<sup>6</sup>-Hya1 drastically alters the membrane permeability to CF (Figure 6). It is remarkable the strong effect of the peptide in zwitterionic membranes in the fluid phase (POPC), at rather low  $[P]/[L]$  ratios. Figure 7 shows the percent of leakage after 1800 s (30 min) of peptide injection, before vesicles disruption with Triton X-100. It is interesting to have in mind that the experiments discussed before, DSC, Trp fluorescence, and DLS, were performed after incubating the peptide–lipid samples for 30 min. Hence, the measured CF leakage values, at the end of 30 min (Figure 7), could arise from the structural alteration of the membrane due to peptide binding. As expected, for all membranes, PC, PG, and PC:PG, the leakage is much stronger through fluid membranes than through gel membranes.

Leakage profiles for the six lipid systems seem to be composed of more than one process. For instance, the leakage induced by the peptide in DPPG vesicles is clearly faster at the beginning, as compared to that in DPPC and DPPC:DPPG. For a clearer understanding of the leakage processes, the kinetics profiles were analyzed assuming exponential processes. Accordingly, most of the kinetics could be fit by two exponentials, related to the two processes (1 and 2), characterized by two different time constants,  $t_1$  and  $t_2$  ( $t_1 < t_2$ ):

$$(\%) \text{leakage}(t) = A_1(1 - \exp(-t/t_1)) + A_2(1 - \exp(-t/t_2)) \quad (7)$$

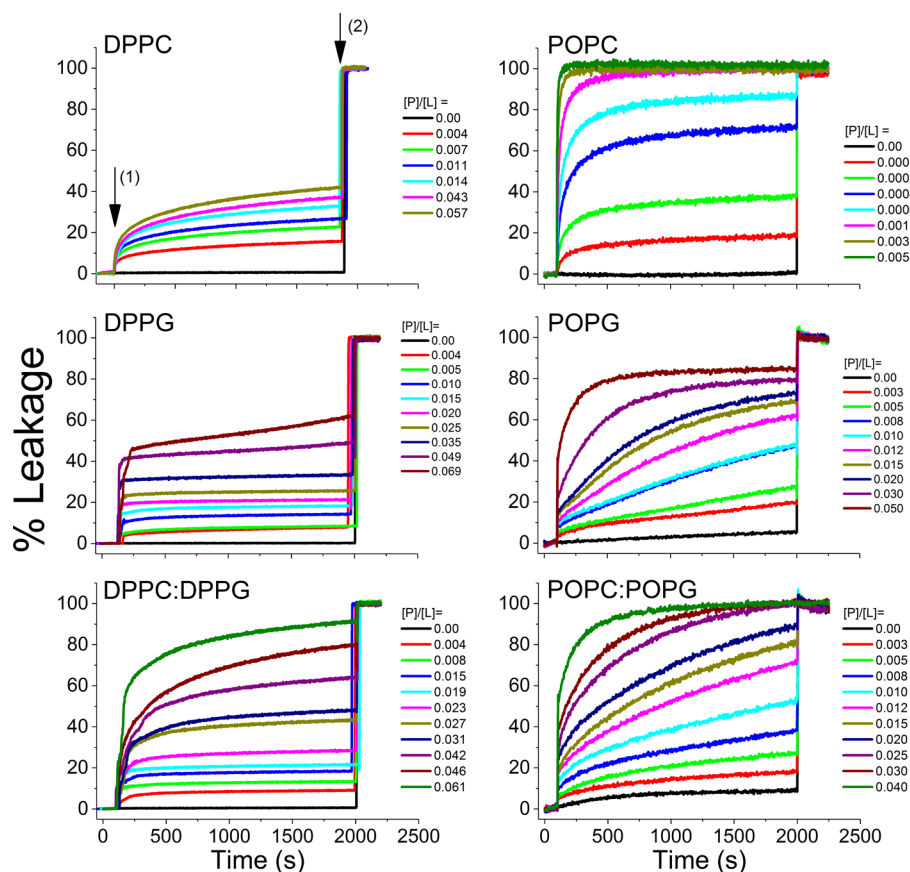


**Figure 6.** Kinetics of CF leakage through LUVs composed of DPPC, DPPG, DPPC:DPPG, POPC, POPG, and POPC:POPG, for different peptide–lipid molar ratios, at  $T = 25$  °C. Black lines correspond to spontaneous leakage ( $\sim 0.5\%$  for DPs and  $\sim 10\%$  for POs), in the absence of peptide. Arrow (1) indicates the moment the peptide was injected, and arrow (2) the moment of surfactant addition.

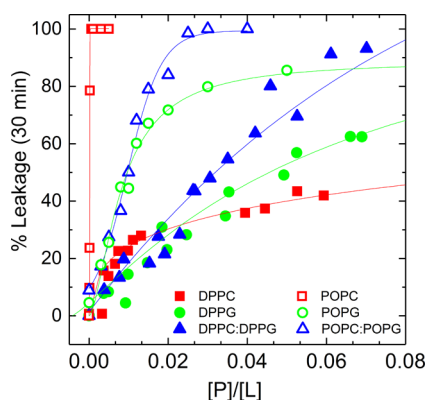


**Figure 7.** Percent of leakage after 30 min of peptide injection, for DPPC and POPC (red squares), DPPG and POPG (green circles), and DPPC:DPPG and POPC:POPG (blue triangles), obtained from Figure 6.

where  $A_1$  and  $A_2$  are the percentage of CF leakage at the end of the processes 1 and 2, which decay with the characteristic times  $t_1$  and  $t_2$ . The total percentage of leakage induced by the peptide is  $A_T = A_1 + A_2$ .

In DPPG, DPPC:DPPG, and POPC, most of the fluorophore leakage happens as soon as the peptide solution is injected in the lipid dispersions, hence related to process 1, whereas for DPPC nearly equal leakage happens at the two processes (see Figure S10). That occurs for all  $[P]/[L]$  ratios studied, as shown in Figure 8, where  $A_1/A_T$  values (relative

leakage in process 1) are plotted as a function of  $[P]/[L]$  ratios. (Figure 8 shows values obtained from fittings of the leakage kinetics with eq 7 which yielded  $R^2 \geq 0.987$  for DPs and  $R^2 \geq 0.8$  for POs, where  $R^2 \equiv$  coefficient of determination.)

Time constants for the two processes are also quite different for the different vesicles. Through gel membranes, the sharp release of CF upon peptide injection in DPPG dispersions is consistent with the short  $t_1$  values obtained from the fittings, around 10 s, compared to  $\sim 40$  s for DPPC dispersions. Values obtained for  $t_2$  are also smaller for DPPG ( $\sim 400$  s) as compared to DPPC ( $\sim 800$  s). For the lipid mixture dispersion, DPPC:DPPG,  $t_2$  values are distributed among those obtained with DPPC and DPPG vesicles, and  $t_1$  values are similar to those obtained with DPPG for low  $[P]/[L]$  ratios, up to around 0.02, and close to those of DPPC for higher peptide concentrations.

For fluid PC membrane,  $t_1$  values are significantly shorter than those obtained for PC in the gel phase, but are somewhat longer than those obtained with fluid anionic membranes. Leakage through fluid and gel phases of PG bilayers display similar  $t_1$  values.

#### 4. DISCUSSION

Considering the preferential activity of antimicrobial peptides against anionic membranes of bacteria as compared to the zwitterionic outer surface of membranes of eukaryotic cells, the present work examined the interaction of the antimicrobial peptide  $K^0$ -W<sup>6</sup>-Hya1 with zwitterionic and anionic lipid vesicles using different techniques.

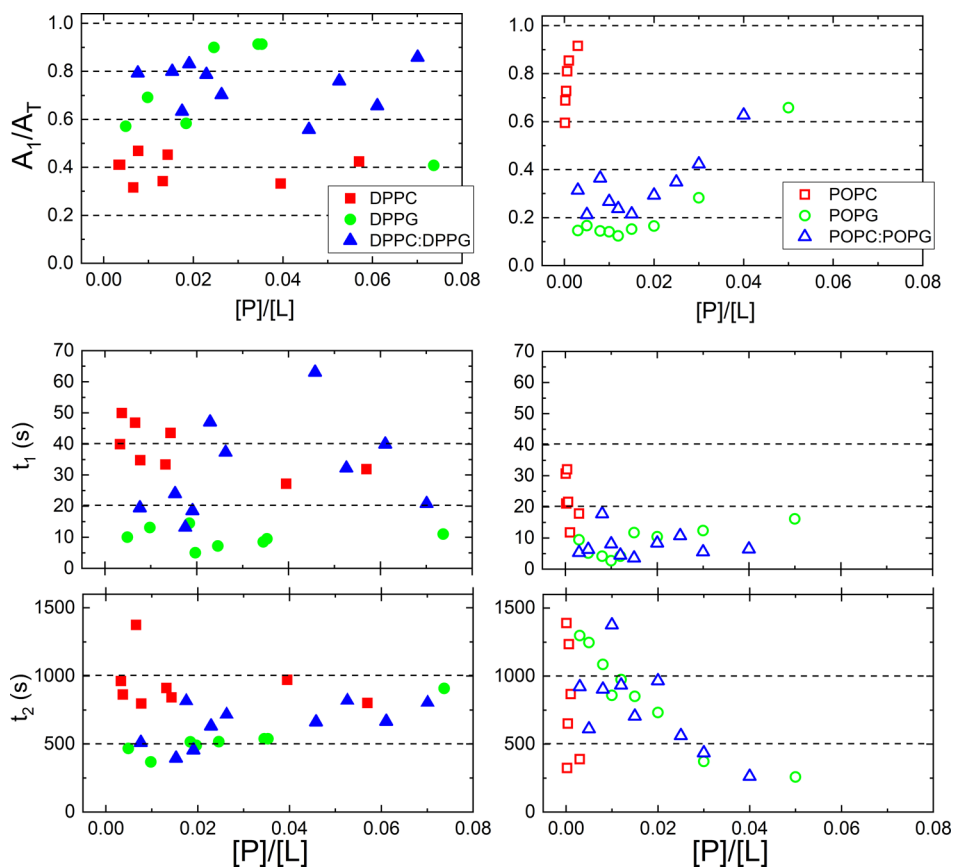


**Figure 8.** Relative total leakage percentage from process 1 ( $A_1/A_T$ ), and time constants,  $t_1$  and  $t_2$ , as a function of  $[P]/[L]$  ratios, obtained by fitting the kinetics of CF leakage (Figure 6) through DPPC and POPC (red squares), DPPG and POPG (green circles), and DPPC:DPPG and POPC:POPG (blue triangles) vesicles, according to eq 7.

Due to the four positive charges of the peptide, one would expect different behavior for the peptide in zwitterionic and anionic lipid dispersions. Indeed,  $K^0$ -W<sup>6</sup>-Hya1 seems to be laterally diffusing in DPPC vesicles, causing a time-average or space-average effect in the bilayer DSC profile (Figure 1). The peptide lateral diffusion seems to happen in the gel and fluid phases of the membrane, as DSC profiles are fairly reversible (Figures 2 and S5). Opposite to that, in DPPG and DPPC:DPPG membranes, DSC profiles suggest the presence of peptide–lipid domains in both the gel and fluid phases of the bilayer. In these membranes,  $K^0$ -W<sup>6</sup>-Hya1 seems to be strongly attached to the membrane, creating a stable peptide-disturbed lipid region, which displays a gel–fluid transition at lower temperatures, as compared with bulk lipid. For low  $[P]/[L]$  ratios, peptide-disturbed domains coexist with bulk lipid bilayer (Figure 1), indicating the slow diffusion of the peptide in negatively charged bilayers.  $K^0$ -W<sup>6</sup>-Hya1 position in the bilayer would be stabilized by the interaction of its two positive termini with PG<sup>−</sup> groups at the surface of the membrane. The peptide effect in anionic membranes could be similar to the known effect of random and frozen defects in liquid crystal systems, where they introduce a random-quenched disorder, resulting in the appearance of a phase transition at lower temperatures.<sup>31,32</sup> This lower temperature transition, caused by the defect-induced disorder, coexists with the usual liquid-crystal phase transition, yielding a DSC profile similar to those found for  $K^0$ -W<sup>6</sup>-Hya1 in anionic membranes.

The coexistence of two peaks in DSC profiles of peptide–lipid membranes has been reported before. For instance, the

coexistence of peptide-depleted and peptide-rich lipid domains was detected in the interaction of the antimicrobial peptide LF11–322RR with DPPG membranes.<sup>33</sup> This is a highly positive charged peptide (+7, with 11 residues), derived from lactoferrin (LF; LF11 corresponds to LF residues 21–31), hence it is probably located at the surface of the membrane, with a strong electrostatic interaction with the phosphate groups. Like the results obtained here with  $K^0$ -W<sup>6</sup>-Hya1, the LF11-322RR-rich DPPG bilayer region yielded an endothermic peak at a temperature lower than that obtained with bulk lipids. SAXS data suggested that this peptide promotes a significant bilayer thinning.<sup>33</sup> On the other hand, an antimicrobial peptide from the magainin family, PGLa, a 21 residues peptide, with five positive charges, displayed a DSC profile where there is a coexistence of two peaks, but the peptide-disturbed thermal event comes at higher temperatures, as compared to the bulk lipid gel–fluid transition.<sup>34</sup> Based on SAXS results, it was proposed that this peptide penetrates the fluid phase of DPPG bilayer, increasing the thickness of the bilayer peptide-rich region, stretching the lipids around the peptide.

The effect of  $K^0$ -W<sup>6</sup>-Hya1 in DPPG DSC profile is similar to that of LF11-322RR, though the latter is a much polar peptide than  $K^0$ -W<sup>6</sup>-Hya1. We know that  $K^0$ -W<sup>6</sup>-Hya1 penetrates anionic lipids, as Trp, at the seventh position of the sequence is found in a rather hydrophobic environment, displaying a  $\Delta\lambda_{\max} \approx 27$  nm, for both gel and fluid phases of the membrane (Figure 4C and D). The similarity between the water-membrane shifts obtained for Trp in DPPG and DPPC:DPPG membranes strongly suggests the induction of a rich DPPG-

domain by the peptide in mixed bilayers composed of DPPC and DPPG, both in the gel and fluid phases of the membrane. That is supported by DSC results, which also indicate similar behavior for the peptide in both anionic membranes (Figures 1 and 2). It is important to have in mind that, due to the nonpolar character of most of K<sup>0</sup>-W<sup>6</sup>-Hya1 midsequence residues, the existence of a barrel stave polar pore formed by K<sup>0</sup>-W<sup>6</sup>-Hya1 molecules only is highly unlikely.

In both gel and fluid phases of DPPG membranes, the fluorescence spectrum of the Trp residue strongly suggests that as K<sup>0</sup>-W<sup>6</sup>-Hya1 concentration increases, and the total [P]/[L] ratio raises from 0.01 to 0.07, the peptide stays almost all bound to anionic vesicles (PG). In contrast, for zwitterionic PC dispersions, the relative concentration of free peptide in the aqueous medium gradually increases as [P]/[L] increases. That conclusion is drawn based on identical fluorescence spectra for K<sup>0</sup>-W<sup>6</sup>-Hya1 in PG and PC:PG dispersions, independently of the peptide concentration and the temperature, and the observed spectrum red shift for the peptide in PC dispersions, as [P]/[L] increases (Figure 4C and D). It is important to mention that results very similar to those obtained with the fluid phase of DPs vesicles (50 °C in Figure 4D) were obtained with the peptide in similar POs vesicles (25 °C in Figure S11).

K<sup>0</sup>-W<sup>6</sup>-Hya1 binds to zwitterionic PC bilayers, with Trp penetrating into a relatively hydrophobic membrane domain, mainly in the fluid phase of the bilayer. That is in accord with the highly hydrophobic character of the peptide, due to several nonpolar residues, including Trp, from the 2nd to the 13th position of the chain. Looking at the wavelength of maximal emission at [P]/[L] = 0.01 (Figure 4D), which is the peptide concentration one would expect the highest fraction of peptide bound in the membrane, due to the lowest positive charge of the peptide-bound membrane, we find  $\Delta\lambda_{\max} \approx 22$  nm for DPPC fluid phase, a significant blue shift from water solution to membrane. For instance, this shift is much larger than those found for Trp in cationic melanotropic peptides bound to fluid anionic vesicles,  $\Delta\lambda_{\max} = 5$  nm for  $\alpha$ -MSH ( $\alpha$ -melanocyte-stimulating hormone)<sup>30,35</sup> or 7 and 13 nm, for the  $\alpha$ -MSH analogues, MSH-I and MSH-II.<sup>30</sup> Moreover, for the melanotropic peptides, no peptide-bound could be detected in zwitterionic vesicles, indicating the major electrostatic character of the interaction. Despite the large blue shift observed in the fluorescent spectrum of K<sup>0</sup>-W<sup>6</sup>-Hya1 in DPPC in the fluid phase, its effect on the DSC profile of zwitterionic bilayers (Figure 1) is very similar to that observed for melanotropic peptides in anionic dispersions.<sup>35</sup> a continuous broadening of the bilayer gel–fluid transition as the peptide concentration increases. Hence, as suggested for melanotropins, K<sup>0</sup>-W<sup>6</sup>-Hya1 seems to be laterally diffusing on DPPC membranes, causing an average and homogeneous effect on the bilayer packing.

In parallel with K<sup>0</sup>-W<sup>6</sup>-Hya1 binding and penetrating zwitterionic PC vesicles, leakage of CF experiments showed that the structure of the membrane of fluid PC vesicles (POPC) is drastically altered by the peptide, with small peptide concentrations causing a quick and full CF leakage (Figure 6). Considering the diffusion of K<sup>0</sup>-W<sup>6</sup>-Hya1 in DPPC bilayers, indicated by DSC data, and the huge leakage observed for fluid membranes, as compared to gel-phase bilayers, a possible mechanism for pores formation in zwitterionic membranes is that proposed by Bechinger,<sup>36</sup> where peptides diffuse on the membrane, surrounded by areas of irregular lipid packing, causing transient openings of pores when these zones overlap. That would explain the enormous increase in CF leakage

observed for the fluid phase of PC vesicles (Figure 7), as the lateral diffusion of lipids in fluid membranes is around 2 orders of magnitude faster than that observed in gel membranes,<sup>37</sup> and one expects that peptide diffusion would be modulated by the lipid diffusion. It is important to have in mind that biological membranes can be rather viscous and/or organized, with cholesterol, sphingolipids, glycolipids, and proteins. For instance, cholesterol in fluid lipid bilayers was found to decrease the translational diffusion coefficient of lipids of 1 order of magnitude, and spatially ordered lipids were found to decrease the diffusion coefficient even further, by 2 orders of magnitude.<sup>37</sup> Hence, one must be cautious about directly relating CF leakage experiments through lipid liposomes with the effect the peptide causes in biological membranes, as the latter are much more complex.

DSC and Trp fluorescence clearly show the different structural mechanisms involved in the binding of K<sup>0</sup>-W<sup>6</sup>-Hya1 to zwitterionic and anionic membranes. Based on the data, Figure 9 shows possible models for K<sup>0</sup>-W<sup>6</sup>-Hya1 in the

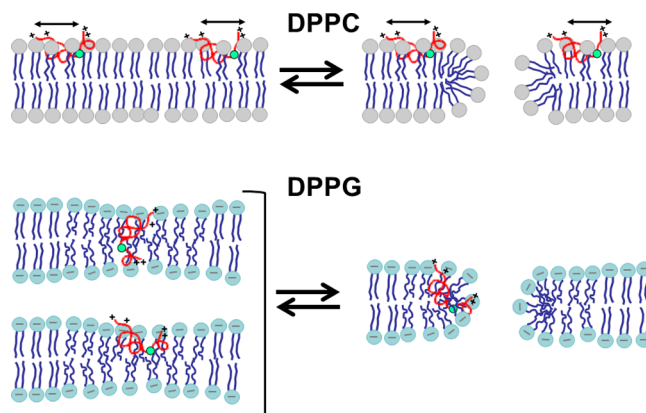


**Figure 9.** Models to illustrate the different binding of K<sup>0</sup>-W<sup>6</sup>-Hya1 in the gel phase of zwitterionic (DPPC) and anionic (DPPG) membranes. In DPPC, K<sup>0</sup>-W<sup>6</sup>-Hya1 is located close to the bilayer surface, allowing peptide diffusion over the surface, and inducing the opening of transient polar pores. In DPPG, the peptide can be at the surface or in a transmembrane position, thinning and disrupting the bilayer around it, inducing stable or transient pores.

membranes, considering the presence of a certain amount of  $\alpha$  helix structure.<sup>15</sup> In PC bilayers, the peptide would diffuse close to the bilayer surface, with the two positive termini at the membrane surface, and the long sequence (13 residues) of nonpolar residues, from Ile<sup>1</sup> to Leu<sup>13</sup>, embedded into the bilayer, with the eventual opening of transient membrane polar pores, large enough to allow CF leakage. In PG bilayers, it is interesting to point out that the large blue shift in the Trp spectrum displayed by K<sup>0</sup>-W<sup>6</sup>-Hya1 is like those found for transmembrane peptides.<sup>32–35</sup> Accordingly, in Figure 9, a possible transmembrane model for the peptide in DPPG bilayer is sketched. Then, the sequence of 13 nonpolar residues, between Ile<sup>1</sup> and Leu<sup>13</sup>, would be embedded into the membrane hydrophobic core, and the bilayer would be squeezed, becoming thinner due to peptide accommodation. This would increase the probability of opening of pores, which could be transient or stable. However, the peptide could also be at the bilayer surface, with the Trp residue deep into the bilayer, and induce membrane curvature, forcing the opening of pores, as shown in Figure 9 for DPPG. In Figure 9, the gel phase of the membranes is sketched.

Though the molecular mechanisms of CF leakage through PC and PG bilayers seem to be quite different, for both systems, CF kinetics of leakage could be modeled by a biexponential process, with two time constants,  $t_1$  and  $t_2$ . In PG membranes, the time constant of the fastest process,  $t_1$ , is rather similar in the two bilayer phases, around 10 s (green circles in Figure 8). However, the fastest process clearly predominates in the bilayer gel phase ( $A_1/A_T \sim 0.7$ ), but not in the fluid phase of the membrane ( $A_1/A_T \sim 0.2$ ). Recently, similar assays with the antimicrobial peptide gomesin and analogues<sup>38</sup> were rationalized considering that the two time constants were related to CF leaking faster at the beginning of the kinetics from a single vesicle, or a small aggregate, and leakage becoming progressively slower as the number of vesicles in an aggregate increases. However, different from the peptide  $K^0$ - $W^6$ -Hya1 studied here, gomesin and its analogues cause a huge increase in light scattering, indicating the formation of large vesicle aggregates.<sup>38</sup> Hence, the two mechanisms found for  $K^0$ - $W^6$ -Hya1, characterized by  $t_1$  and  $t_2$  values, are still a matter of investigation.

In PG membranes, both gel and fluid, one could speculate that the faster process is related to the peptide binding to the membrane and strongly disturbing the nearby lipids. After a few seconds, the disturbed structure of peptide-bound lipids would stabilize, and the leakage would continue, but slower. That is in accordance with the larger contribution of the faster process for  $K^0$ - $W^6$ -Hya1 in the well packed gel phase of anionic vesicles, considering its penetration into the bilayer core, and the significant disruption it can cause in the gel membrane.

For higher peptide concentrations, there is a significant increase in the leakage through the mixed system DPPC:DPPG as compared to pure DPPG. As DSC and fluorescence experiments indicate that  $K^0$ - $W^6$ -Hya1 is mostly embedded in a DPPG environment, one can attribute this increase in leakage to the relative higher peptide-DPPG ratio in the mixture, and/or to defects caused in DPPC:DPPG bilayers due to the peptide-DPPG segregation.

The above discussion considers the two process that well fit most of the CF leakage kinetics. However, it is important to note that most of the leakage kinetics induced by  $K^0$ - $W^6$ -Hya1, in both PC and PG membranes, level off before achieving 100% of leakage, that is  $A_T = (A_1 + A_2) < 100$  (see Figures 6 and S12 for  $A_T$  values). That happens to many antimicrobial peptides, and has been the subject of discussion in the literature (see, for instance, refs 39 and 40). Though it is still an open question, it was suggested that the leakage is caused by initial non-equilibrium events, probably involving peptide translocation across the bilayer, which would stop after equilibrium is reached. Alternatively, as the total percentage of CF leakage ( $A_T$ ) increases with  $[P]/[L]$  ratio (Figure S12), one could speculate<sup>39</sup> that a certain amount of peptide-bound per vesicle would be necessary for triggering the opening of pores and CF leak, possibly related to peptide–peptide interaction on the membrane. Hence, the CF leakage would not be complete until all vesicles reach this value, and the increase on the peptide concentration would increase the fraction of leaky vesicles. In that case, even in PG membranes, more than one peptide would be necessary for the opening of pores, and not just one as sketched in Figure 9. However, this is still a matter of discussion, and it is being currently investigated with  $K^0$ - $W^6$ -Hya1 and other Hya1 analogues.

## 5. CONCLUSIONS

This work clearly reveals the different structural mechanisms involved in the interaction of the peptide  $K^0$ - $W^6$ -Hya1 with zwitterionic and anionic lipid vesicles.

DSC shows that the peptide is strongly attached to anionic bilayers, giving rise to the coexistence of two different lipid regions, one like bulk lipids and another peptide-disturbed. This contrasts with the peptide diffusion in DPPC membranes. Moreover, in mixed bilayers (DPPC:DPPG), the peptide sequesters negatively charged lipids, creating anionic lipid domains, strongly disturbing the membrane. Trp fluorescence spectroscopy shows that the differences are related to the different partition and penetration of the peptide into zwitterionic and anionic lipid bilayers. The data presented here were rationalized assuming that the peptide is located at the surface of zwitterionic vesicles, laterally diffusing on it, triggering the opening of transient membrane polar pores due to the overlapping of irregular lipid packing zones, as suggested by Bechinger.<sup>36</sup> In contrast, in anionic bilayers,  $K^0$ - $W^6$ -Hya1 would be deeply embedded and attached to the bilayer, probably in a transmembrane position, inducing stable or transient polar pores. As discussed, more experiments are necessary to try to reveal the whole mechanism of  $K^0$ - $W^6$ -Hya1 membrane-binding and the cease of leakage before the complete loss of entrapped contents.

Though one needs to be cautious in extending the results with simple membrane models to biological membranes, the distinct interactions displayed by  $K^0$ - $W^6$ -Hya1 in PC and PG membranes are probably related to the different mechanisms of action of the peptide in anionic prokaryotic and zwitterionic eukaryotic cell membranes.

## ■ ASSOCIATED CONTENT

### Supporting Information

The Supporting Information is available free of charge on the ACS Publications website at DOI: 10.1021/acs.langmuir.7b03408.

Two tables with  $T_m$ ,  $T_p$ , and  $\Delta H$  values; figures related to experiments discussed in the text, but not shown (PDF)

## ■ AUTHOR INFORMATION

### Corresponding Authors

\*Tel: +55 11 30916829. E-mail: mtlamy@if.usp.br.

\*Tel: 607-379-4532. E-mail: ta327@cornell.edu.

### ORCID

Eduardo M. Cilli: 0000-0002-4767-0904

Karin A. Riske: 0000-0003-4080-1358

M. Teresa Lamy: 0000-0001-6616-6546

### Present Address

<sup>†</sup>T.A.E.: Department of Molecular Biology and Genetics, Cornell University, Ithaca, NY, USA.

### Author Contributions

T.A.E. performed the experiments with saturated lipids. I.M.-S. performed the experiments with unsaturated lipids. E.N.L. and E.M.C. synthesized the peptide  $K^0$ - $W^6$ -Hya1. T.A.E., K.R.P., K.A.R., and M.T.L. designed the research, analyzed the data, and cowrote the manuscript.

### Notes

The authors declare no competing financial interest.

## ACKNOWLEDGMENTS

This work was supported by USP, FAPESP (2013/14419-3) and CNPq. T.A.E. thanks FAPESP for a Ph.D. fellowship (2010/11671-5), and I.M.-S. thanks a Ph.D. fellowship from CNPq. E.M.C., K.R.P., K.A.R., and M.T.L. acknowledge research fellowships from CNPq. T.A.E. and M.T.L. thank Carla Goldman for helpful discussions.

## ABBREVIATIONS

AMP antimicrobial peptide  
 CF carboxyfluorescein  
 DLS dynamic light scattering  
 DPPC 1,2-dipalmitoyl-*sn*-glycero-3-phosphocholine  
 DPPG 1,2-dipalmitoyl-*sn*-glycero-3-phospho-(1'-*rac*-glycerol) - sodium salt  
 DPs 1,2-dipalmitoyl lipids  
 DSC differential scanning calorimetry  
 HEPES 4-(2-hydroxyethyl)-1-piperazineethanesulfonic acid  
 K<sup>0</sup>-W<sup>6</sup>-Hya1 antimicrobial peptide K<sup>0</sup>-W<sup>6</sup>-Hylin a1 analogue  
 POPC 1-palmitoyl-2-oleoyl-*sn*-glycero-3-phosphocholine  
 POPG 1-palmitoyl-2-oleoyl-*sn*-glycero-3-phospho-(1'-*rac*-glycerol) - sodium salt  
 POs 1-palmitoyl-2-oleoyl lipids  
 T<sub>p</sub> pretransition temperature  
 T<sub>m</sub> main-transition temperature

## REFERENCES

- Yeaman, M. R.; Yount, N. Y. Mechanisms of Antimicrobial Peptide Action and Resistance. *Pharmacol. Rev.* **2003**, *55* (1), 27–55.
- Zasloff, M. Antimicrobial Peptides of Multicellular Organisms. *Nature* **2002**, *415*, 389–395.
- World Health Organization. *The Evolving Threat of Antimicrobial Resistance - Options for Action*; Martinez, L., Ed.; World Health Organization GPS Publishing, 2012.
- He, K.; Ludtke, S. J.; Worcester, D. L.; Huang, H. W. Neutron Scattering in the Plane of Membranes: Structure of Alamethicin Pores. *Biophys. J.* **1996**, *70* (6), 2659–2666.
- Yang, L.; Harroun, T. A.; Weiss, T. M.; Ding, L.; Huang, H. W. Barrel-Stave Model or Toroidal Model? A Case Study on Melittin Pores. *Biophys. J.* **2001**, *81* (3), 1475–1485.
- Dufourc, E. J.; Smith, I. C. P.; Dufourcq, J. Molecular Details of Melittin-Induced Lysis of Phospholipid Membranes as Revealed by Deuterium and Phosphorus NMR. *Biochemistry* **1986**, *25* (21), 6448–6455.
- Pott, T.; Dufourc, E. J. Action of Melittin on the DPPC-Cholesterol Liquid-Ordered Phase: A Solid State 2H-and 31P-NMR Study. *Biophys. J.* **1995**, *68* (3), 965–977.
- Latal, A.; Degovics, G.; Epanand, R. F.; Epanand, R. M.; Lohner, K. Structural Aspects of the Interaction of Peptidyl-Glycylleucine-Carboxamide, a Highly Potent Antimicrobial Peptide from Frog Skin, with Lipids. *Eur. J. Biochem.* **1997**, *248* (3), 938–946.
- Joanne, P.; Galanth, C.; Goasdoué, N.; Nicolas, P.; Sagan, S.; Lavielle, S.; Chassaing, G.; El Amri, C.; Alves, I. D. Lipid Reorganization Induced by Membrane-Active Peptides Probed Using Differential Scanning Calorimetry. *Biochim. Biophys. Acta, Biomembr.* **2009**, *1788* (9), 1772–1781.
- Aroui, A.; Dathe, M.; Blume, A. Peptide Induced Demixing in PG/PE Lipid Mixtures: A Mechanism for the Specificity of Antimicrobial Peptides towards Bacterial Membranes? *Biochim. Biophys. Acta, Biomembr.* **2009**, *1788* (3), 650–659.
- Epanand, R. M.; Rotem, S.; Mor, A.; Berno, B.; Epanand, R. F. Bacterial Membranes as Predictors of Antimicrobial Potency. *J. Am. Chem. Soc.* **2008**, *130* (43), 14346–14352.
- El Jastimi, R.; Lafleur, M. Nisin Promotes the Formation of Non-Lamellar Inverted Phases in Unsaturated Phosphatidylethanolamines. *Biochim. Biophys. Acta, Biomembr.* **1999**, *1418* (1), 97–105.
- Yang, L.; Gordon, V. D.; Mishra, A.; Som, A.; Purdy, K. R.; Davis, M. A.; Tew, G. N.; Wong, G. C. L. Synthetic Antimicrobial Oligomers Induce a Composition-Dependent Topological Transition in Membranes. *J. Am. Chem. Soc.* **2007**, *129* (40), 12141–12147.
- Riske, K. A. Optical Microscopy of Giant Vesicles as a Tool to Reveal the Mechanism of Action of Antimicrobial Peptides and the Specific Case of Gomesin. *Adv. Planar Lipid Bilayers Liposomes* **2015**, *21*, 99–129.
- Crusca, E.; Rezende, A. a; Marchetto, R.; Mendes-Giannini, M. J. S.; Fontes, W.; Castro, M. S.; Cilli, E. M. Influence of N-Terminus Modifications on the Biological Activity, Membrane Interaction, and Secondary Structure of the Antimicrobial Peptide Hylin-a1. *Biopolymers* **2011**, *96* (1), 41–48.
- da Silva, B. R.; de Freitas, V. A. A.; Carneiro, V. A.; Arruda, F. V. S.; Lorenzón, E. N.; de Aguiar, A. S. W.; Cilli, E. M.; Cavada, B. S.; Teixeira, E. H. Antimicrobial Activity of the Synthetic Peptide Lys-a1 against Oral Streptococci. *Peptides* **2013**, *42*, 78–83.
- Castro, M. S.; Ferreira, T. C. G.; Cilli, E. M.; Crusca, E.; Mendes-Giannini, M. J. S.; Sebben, A.; Ricart, C. A. O.; Sousa, M. V.; Fontes, W. Hylin a1, the First Cytolytic Peptide Isolated from the Arboreal South American Frog *Hypsiboas Albolopuncatus* (“spotted Treefrog”). *Peptides* **2009**, *30* (2), 291–296.
- Manzini, M. C.; Perez, K. R.; Riske, K. A.; Bozelli, J. C.; Santos, T. L.; da Silva, M. A.; Saraiva, G. K. V.; Politi, M. J.; Valente, A. P.; Almeida, F. C. L.; et al. Peptide:lipid Ratio and Membrane Surface Charge Determine the Mechanism of Action of the Antimicrobial Peptide BP100. Conformational and Functional Studies. *Biochim. Biophys. Acta, Biomembr.* **2014**, *1838* (7), 1985–1999.
- Rouser, G.; Siakotos, A. N.; Fleischer, S. Quantitative Analysis of Phospholipids by Thin-Layer Chromatography and Phosphorus Analysis of Spots. *Lipids* **1966**, *1* (1), 85–86.
- Riske, K. A.; Barroso, R. P.; Vequi-Suplicy, C. C.; Germano, R.; Henriques, V. B.; Lamy, M. T. Lipid Bilayer Pre-Transition as the Beginning of the Melting Process. *Biochim. Biophys. Acta, Biomembr.* **2009**, *1788* (5), 954–963.
- Valeur, B. *Molecular Fluorescence: Principles and Applications*, Second ed.; Wiley, 2001.
- Tucker, S. A.; Amszi, V. L.; Acree, W. E. Primary and Secondary Inner Filtering. Effect of K2Cr2O7 on Fluorescence Emission Intensities of Quinine Sulfate. *J. Chem. Educ.* **1992**, *69* (1), A8.
- Mendonça, A.; Rocha, A. C.; Duarte, A. C.; Santos, E. B. H. The Inner Filter Effects and Their Correction in Fluorescence Spectra of Salt Marsh Humic Matter. *Anal. Chim. Acta* **2013**, *788*, 99–107.
- Berne, B.; Pecora, R. *Dynamic Light Scattering: With Applications to Chemistry, Biology, and Physics*; Dover Publications: New York, 2000.
- Koppel, D. E. Analysis of Macromolecular Polydispersity in Intensity Correlation Spectroscopy: The Method of Cumulants. *J. Chem. Phys.* **1972**, *57* (11), 4814.
- Enoki, T. A.; Henriques, V. B.; Lamy, M. T. Light Scattering on the Structural Characterization of DMPG Vesicles along the Bilayer Anomalous Phase Transition. *Chem. Phys. Lipids* **2012**, *165* (8), 826–837.
- Martins, R. M.; Amino, R.; Daghasanli, K. R.; Cuccovia, I. M.; Juliano, M. A.; Schenkman, S. A Short Proregion of Trialysin, a Pore-Forming Protein of *Triatoma Infestans* Salivary Glands, Controls Activity by Folding the N-Terminal Lytic Motif. *FEBS J.* **2008**, *275* (5), 994–1002.
- Heimburg, T. *Thermal Biophysics of Membranes; Tutorials in Biophysics*; Wiley-VCH Verlag GmbH & Co. KGaA: Weinheim, Germany, 2007.
- Cantor, C. R.; Schimmel, P. R. *Techniques for the Study of Biological Structure and Function*, first ed.; W.H. Freeman and Company: New York, 1980.
- Ito, A. S.; Castrucci, A. M.; Hruby, V. J.; Hadley, M. E.; Krajcarski, D. T.; Szabo, A. G. Structure-Activity Correlations of Melanotropin Peptides in Model Lipids by Tryptophan Fluorescence Studies. *Biochemistry* **1993**, *32* (45), 12264–12272.
- Crucenau, F.; Liang, D.; Leheny, R. L.; Iannacchione, G. S. Calorimetric study of the isotropic to nematic phase transition in an

aligned liquid crystal nano-colloidal gel. *Liq. Cryst.* **2008**, *35* (9), 1061–1071.

(32) Zammit, U.; Marinelli, M.; Mercuri, F.; Paoloni, S. Effect of Confinement and Strain on the Specific Heat and Latent Heat over the Nematic-Isotropic Phase Transition of 8CB Liquid Crystal. *J. Phys. Chem. B* **2009**, *113* (43), 14315–14322.

(33) Zweytick, D.; Japelj, B.; Mileykovskaya, E.; Zorko, M.; Dowhan, W.; Blondelle, S. E.; Riedl, S.; Jerala, R.; Lohner, K. N-Acylated Peptides Derived from Human Lactoferricin Perturb Organization of Cardiolipin and Phosphatidylethanolamine in Cell Membranes and Induce Defects in Escherichia Coli Cell Division. *PLoS One* **2014**, *9* (3), e90228.

(34) Pabst, G.; Grage, S. L.; Danner-Pongratz, S.; Jing, W.; Ulrich, A. S.; Watts, A.; Lohner, K.; Hickel, A. Membrane Thickening by the Antimicrobial Peptide PGLa. *Biophys. J.* **2008**, *95* (12), 5779–5788.

(35) Contreras, L. M.; de Almeida, R. F.; Villalaín, J.; Fedorov, A.; Prieto, M. Interaction of Alpha-Melanocyte Stimulating Hormone with Binary Phospholipid Membranes: Structural Changes and Relevance of Phase Behavior. *Biophys. J.* **2001**, *80* (5), 2273–2283.

(36) Bechinger, B. The Structure, Dynamics and Orientation of Antimicrobial Peptides in Membranes by Multidimensional Solid-State NMR Spectroscopy. *Biochim. Biophys. Acta, Biomembr.* **1999**, *1462*, 157–183.

(37) Korlach, J.; Schwille, P.; Webb, W. W.; Feigenson, G. W. Characterization of Lipid Bilayer Phases by Confocal Microscopy and Fluorescence Correlation Spectroscopy. *Proc. Natl. Acad. Sci. U. S. A.* **1999**, *96*, 8461–8466.

(38) Mattei, B.; Miranda, A.; Perez, K. R.; Riske, K. A. Structure-Activity Relationship of the Antimicrobial Peptide Gomesin: The Role of Peptide Hydrophobicity in Its Interaction with Model Membranes. *Langmuir* **2014**, *30* (12), 3513–3521.

(39) Wimley, W. Describing the Mechanism of Antimicrobial Peptide Action with the Interfacial Activity Model. *ACS Chem. Biol.* **2010**, *5* (10), 905–917.

(40) Gregory, S. M.; Cavanaugh, A.; Journigan, V.; Pokorny, A.; Almeida, P. F. F. *Biophys. J.* **2008**, *94*, 1667–1680.

## Supporting Information

### The antimicrobial peptide K<sup>0</sup>-W<sup>6</sup>-Hya1 induces stable structurally modified lipid domains in anionic membranes

Thais A. Enoki, Isabela Moreira-Silva, Esteban N. Lorenzon, Eduardo M. Cilli, Katia R. Perez, Karin A. Riske, M. Teresa Lamy



**Fig. S1.** Sequence of the antimicrobial peptide K<sup>0</sup>-W<sup>6</sup>-Hya1, showing the position of the positive charges, polar (red) and non-polar (black) residues. For clarity, the fluorescent Trp and the helix-breaking Pro are underlined.

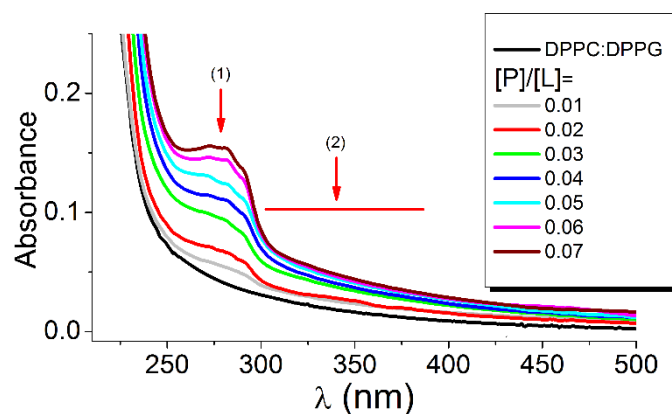


**Fig. S2.** Optical absorption spectra of DPPC:DPPG dispersions at T=50°C (fluid phase of the lipid mixture) with the following peptide-lipid molar ratios: [P]/[L]= 0.01, 0.02, 0.03, 0.04, 0.05, 0.06 and 0.07. Arrows (1) and (2) indicate the absorbance values to be considered in the primary and secondary inner filter corrections, respectively, as discussed in Experimental section.

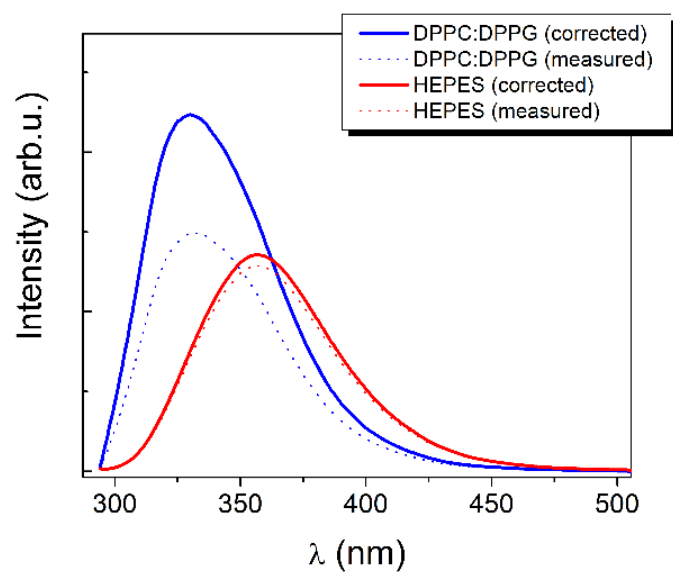


**Figure S3.** Inner filter correction for  $K^0$ -W<sup>6</sup>-Hya1 in lipid dispersion of DPPC:DPPG (blue lines), and in buffer solution (red lines).  $\lambda_{exc}=280$  nm. Measured spectra (dotted lines), and corrected spectra (solid lines), according to Eq. 1.

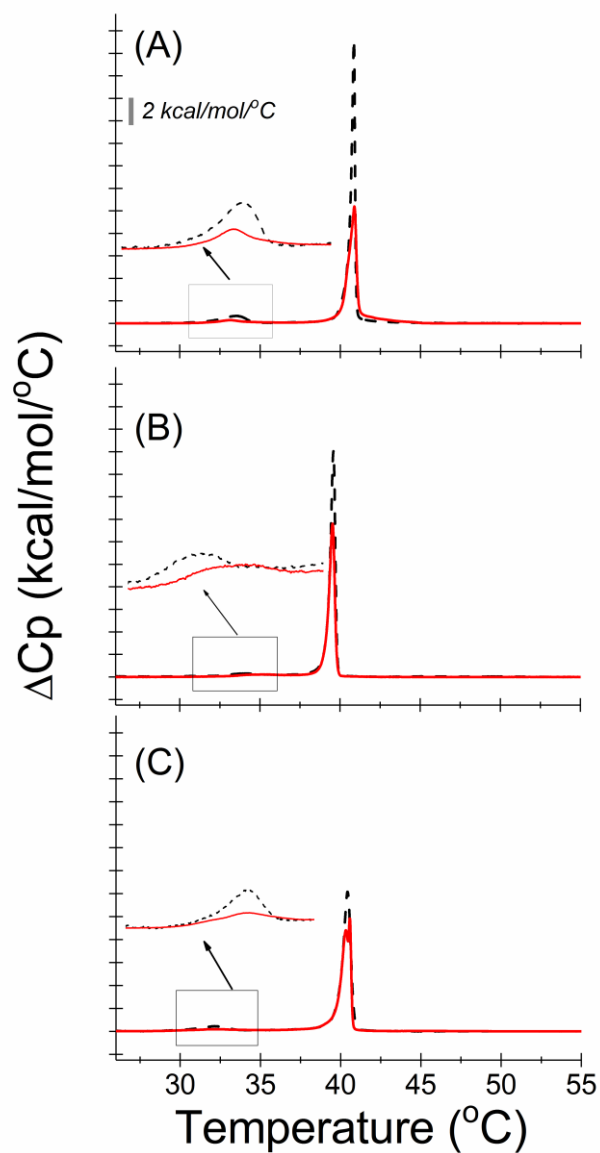


**Figure S4.** Comparison of DSC profiles for non-extruded (dashed black) and extruded (red) DPPC (A), DPPG (B) and DPPC:DPPG (1:1) (C) dispersions. Scans were performed from 15 to 60°C, with a scan rate of 20°C/h. Inserts in the graphs amplify the pre-transition region for each lipid system. In general, extruded vesicles display less cooperative transitions, due to the increase in the bilayer curvature<sup>1</sup>

**Table S1.** Main phase transition temperatures ( $T_m$ ) and enthalpies ( $\Delta H_m$ ), and pre-transition temperatures ( $T_p$ ) and enthalpies ( $\Delta H_p$ ), for the three lipid systems used, extruded and non-extruded.

	$T_p$ (°C)	$\Delta H_p$ (kcal/mol)	$T_m$ (°C)	$\Delta H_m$ (kcal/mol)
DPPC non-extruded	33.7±0.2 (3)	1.4±0.1 (3)	40.9±0.1 (3)	8.4±0.1 (3)
DPPC extruded	33.5±0.1 (2)	0.6±0.1 (2)	41.1±0.1 (2)	8.1±0.6 (2)
DPPG non-extruded	34.8±1.2 (4)	1.1±0.1 (4)	39.5±0.2 (4)	8.4±0.2 (4)
DPPG extruded	34.8±1.2 (4)	0.6±0.1 (3)	39.5±0.1 (3)	8.4±0.2 (3)
DPPC:DPPG non-extruded	31.6±0.2 (4)	1.3±0.1 (4)	40.5±0.1 (4)	8.2±0.2 (4)
DPPC:DPPG extruded	32.4±0.4 (3)	0.6±0.1 (3)	40.3±0.7 (3)	7.9±0.2 (3)

The number of measured independent samples is shown in parenthesis.

**Table S2.** . Main phase transition enthalpy values from DSC profiles shown in Figure 1.

[P]/[L]	$\Delta H$ (kcal/mol/°C)		
	DPPC	DPPG	DPPC:DPPG
0.00	8.1 ± 0.1	8.4 ± 0.3	7.9 ± 0.1
0.02	8.1 ± 0.1	7.7 ± 0.2	8.0 ± 0.1
0.03	7.7 ± 0.3	7.8 ± 0.1	8.0 ± 0.1
0.04	7.8 ± 0.3	7.6 ± 0.5	7.98 ± 0.04
0.05	7.6 ± 0.5	7.3 ± 0.1	8.3 ± 0.3
0.07	7.6 ± 0.4	6.3 ± 0.5	8.0 ± 0.2

Standard deviations from at least three different samples are shown.

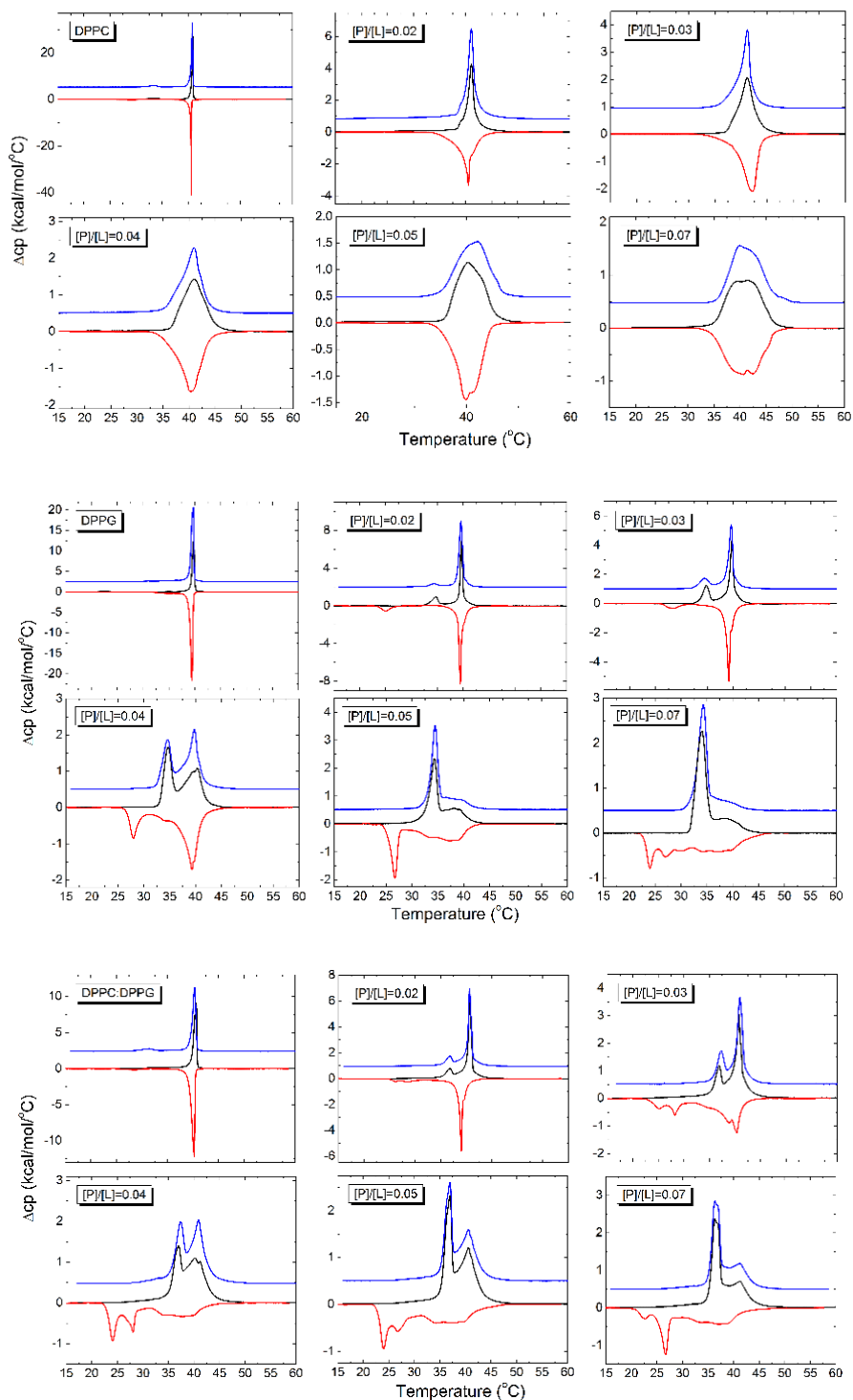


**Figure S5.** Comparison of DSC profiles for DPPC, DPPG and DPPC:DPPG. A temperature up-scan (black) was followed by a temperature down-scan and a second temperature up-scan (blue).

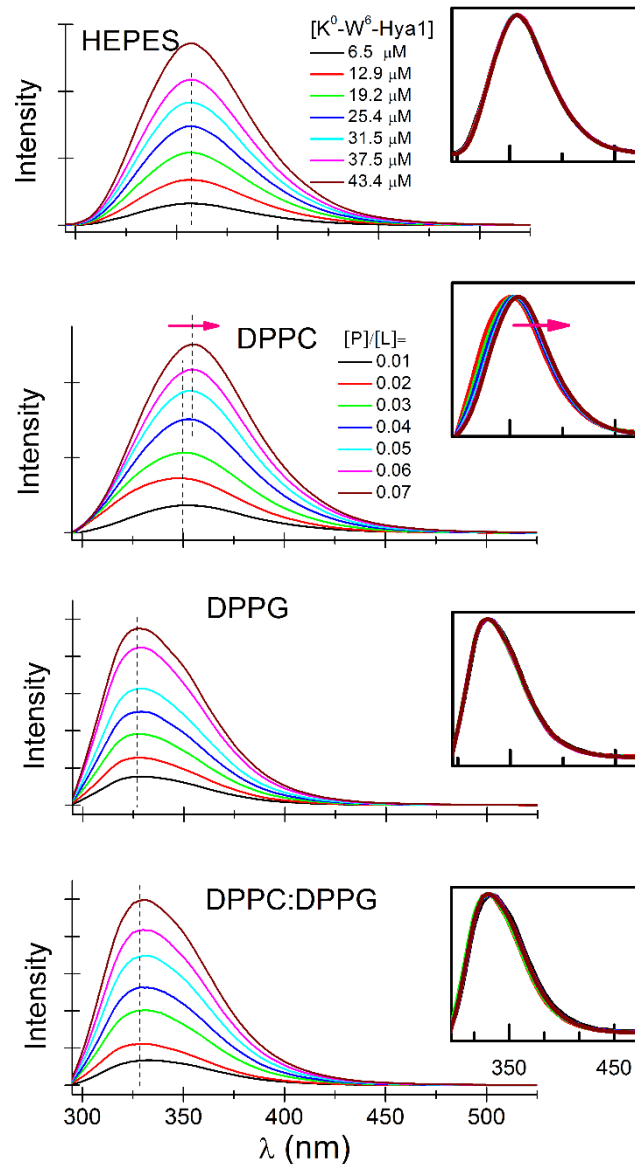


**Figure S6.** Emission spectra of peptide  $K^0-W^6$ -Hya1 in HEPES buffer and in lipid dispersions of DPPC, DPPG and DPPC:DPPG, at the peptide-lipid molar ratios  $[P]/[L] = 0.01, 0.02, 0.03, 0.04, 0.05, 0.06$  and  $0.07$ , at  $T=25^\circ\text{C}$  (membrane gel phase). Spectra were corrected for the inner filter effect as discussed in the Experimental section. Dotted lines indicate the wavelength of maximal emission, and insets show the normalized spectra. The vertical spacing represents 200 a. u. in the intensity axis.

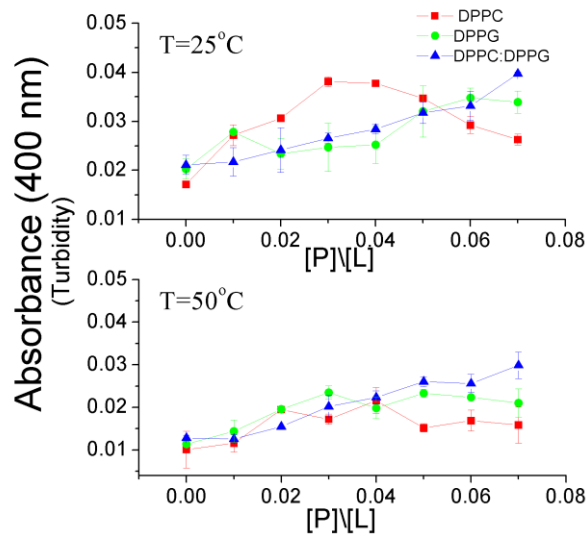


**Figure S7.** Turbidity (Absorbance at 400 nm) of the lipid dispersions as a function of the peptide molar fraction: DPPC (red square), DPPG (green circle) and DPPC:DPPG (blue triangle). Data at T=25°C (membrane gel phase) and T=50°C (membrane fluid phase).

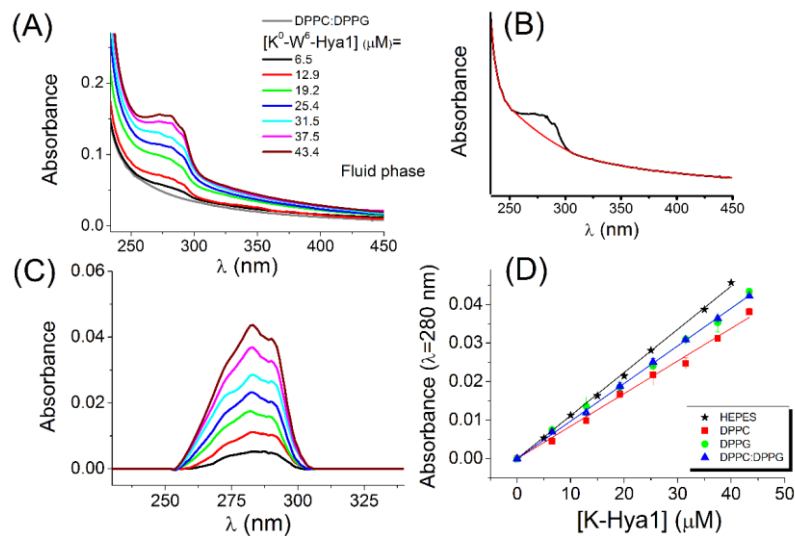


**Figure S8.** The linear dependence of K<sup>0</sup>-W<sup>6</sup>-Hya1 Absorbance at 280nm with peptide concentration, in DPPC:DPPG dispersion (D), measured from the “corrected spectra” (C). These “corrected spectra” focus on the absorption band at 280 nm, hence they are obtained from original absorption spectra (A) after the subtraction of a base line (B). The base line is due to light scattering and peaks at lower wavelength, as it is impossible to separate the two effects. Here T = 50°C, but similar results were obtained for T = 25°C, and for the other two lipid systems, DPPC and DPPG.

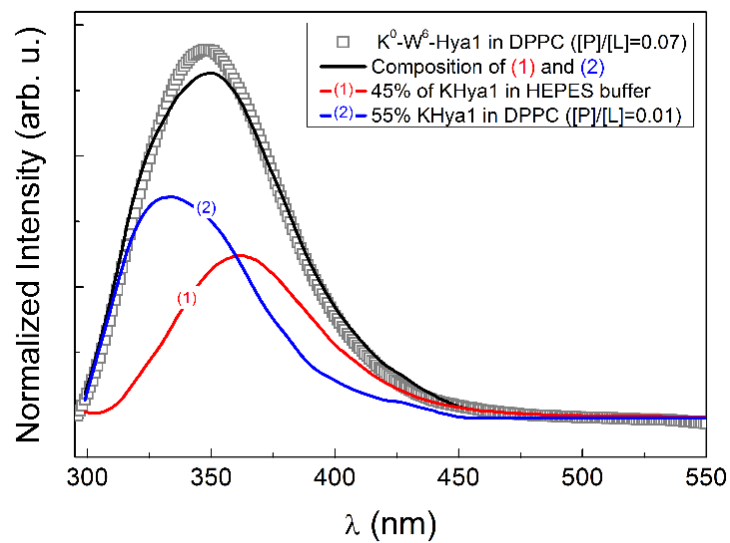


**Figure S9.** Example of a decomposition of the peptide emission spectrum in DPPC dispersion,  $[P]/[L]=0.07$  ( $\square$ ). Solid black line is the sum of 45% of the spectrum measured for the peptide in HEPES (red) and 55% of the spectrum measured for the peptide in DPPC,  $[P]/[L]=0.01$  (blue). Spectra at 50°C.

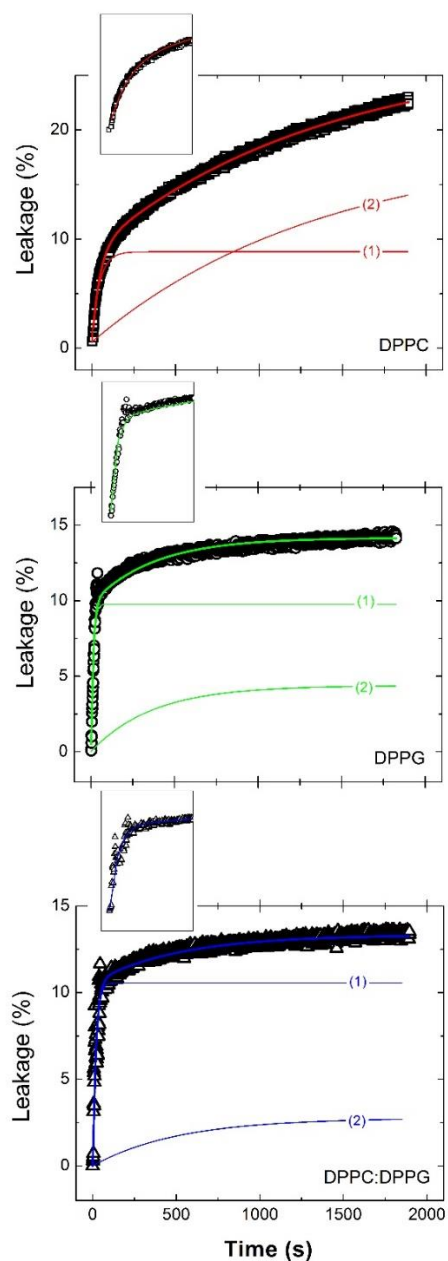


**Figure S10.** Typical fittings of the leakage kinetics according to Eq. (7): DPPC with  $[P]/[L]= 0.07$ ,  $R^2= 0.998$ ; DPPG with  $[P]/[L]= 0.01$ ,  $R^2 = 0.963$ ; and DPPC:DPPG with  $[P]/[L]= 0.08$ ,  $R^2 = 0.965$ . For clarity, Eq. (7) is divided in two parts, (1) corresponds to the fastest process ( $A_1 (1 - \exp(-t/t_1))$ ), and (2) to the slowest process ( $A_2 (1 - \exp(-t/t_2))$ ). The insert in the graphs displays the firsts 200 seconds.

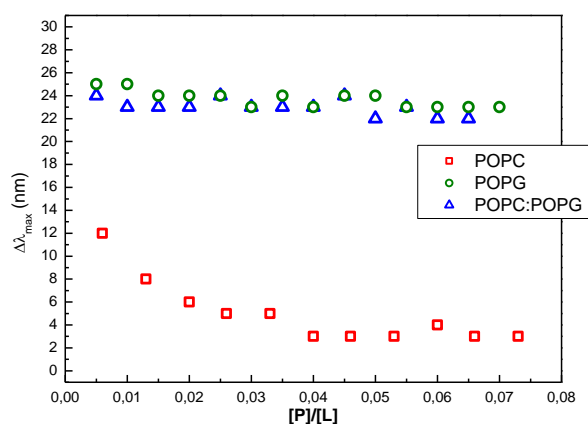


**Figure S11.** Effect of the peptide concentration on the shift of the Trp fluorescent band relative to the band in HEPES ( $\Delta\lambda_{\max}$ ) in lipid dispersions of POPC (red squares), POPG (green circles) and POPC:POPG (blue triangles), at 25°C.  $\lambda_{\text{exc}}=280$  nm.

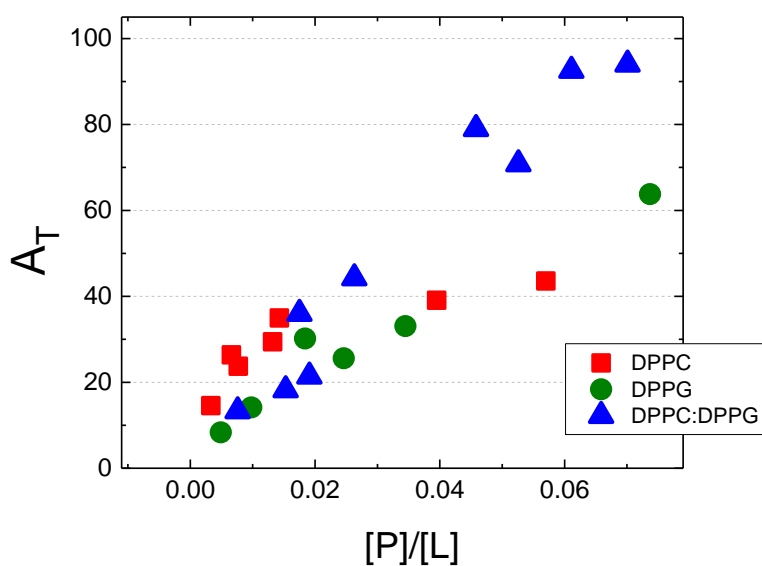


**Figure S12.** The dependence of the total percentage of leakage induced by the peptide,  $A_T = A_1 + A_2$ , on the  $[P]/[L]$  ratio, for DPPC, DPPG and DPPC:DPPG.

## Reference

<sup>1</sup> Heimburg, T. *Thermal Biophysics of Membranes*; Wiley-VCH Verlag GmbH & Co. KGaA: Weinheim, Germany, 2007.